Hydrological Processes

WILEY

RESEARCH ARTICLE OPEN ACCESS

A Novel Technique to Mitigate Saltwater Intrusion: Freshwater Recharge via Drainpipe in Permeable Paleochannels

Ester Zancanaro[1] | Francesco Morari[2] | Ilaria Piccoli[2] | Alberto Carrera[2] | Claudia Zoccarato[1] | Pietro Teatini[1]

[1]Department of Civil, Environmental and Architectural Engineering (ICEA), University of Padova, Padova, Italy | [2]Department of Agronomy, Food, Natural Resources, Animals and Environment (DAFNAE), University of Padova, Legnaro, Italy

Correspondence: Ester Zancanaro (ester.zancanaro@unipd.it)

Received: 19 June 2024 | **Revised:** 14 September 2024 | **Accepted:** 19 September 2024

Funding: This work was supported by Next Generation EU, European Regional Development Fund and Interreg.

Keywords: coastal aquifer | managed aquifer recharge | saltwater contamination | Venice coastland

ABSTRACT

Seawater intrusion (SWI) is threatening coastal aquifers and farmland productivity worldwide. Although this phenomenon naturally occurs in coastal areas, it is intensified by anthropogenic activities such as groundwater pumping and land reclamation that cause a lowering of the hydraulic head and land subsidence. Moreover, the consequences of climate change such as sea level rise, increase of the mean temperature and the shifting of rainfall events to tropical regimes, have strong negative effects on groundwater quality and agriculture. Countermeasures against SWI are needed to maintain agricultural productivity and protect the freshwater resources in coastal areas. In the low-lying farmlands surrounding the southern Venice Lagoon, in northern Italy, SWI is exacerbated by land subsidence, the presence of sandy paleochannels connected to the lagoon subsurface, seawater encroachment into the river estuaries, the presence of fossil brine waters and peat deposits. This study provides a detailed hydrogeological and geochemical characterisation of an experimental agricultural field affected by SWI located in this area using a large dataset collected over the 4 years between 2019 and 2022. Furthermore, it presents the results of novel intervention established across the farmland in 2021 to mitigate saltwater contamination. This intervention involved a controlled discharge of freshwater supplied by a reclamation channel through a 200 m-long drainpipe buried 1.5 m below the field surface along a well-preserved sandy paleochannel. The interpretation of the collected data demonstrates that the freshwater recharge carried out in 2021 and 2022 effectively reduced the groundwater salinity along the paleochannel. Moreover, statistical analyses highlighted that a certain lateral spread of freshwater occurred too, although the variability of the monitored parameters in the sites located outside the sandy body was only partially explained by the drain activity.

1 | Introduction

Coastal aquifers, especially the shallow ones, are globally threatened by seawater intrusion (SWI) that negatively impacts groundwater quality and agricultural production. Although SWI naturally occurs in coastal areas, it is exacerbated by the rise of the world population and the consequent excessive groundwater extraction for both human and agricultural uses, land reclamation and extraction of other natural resources such as oil and gas causing land subsidence (Oude Essink 2001; Zancanaro et al. 2020). SWI is also threatening freshwater resources inland because of the increasing encroachment of saline water from river estuaries (Oude Essink 2001; Prusty and Farooq 2020).

Climate change is intensifying the pressure on groundwater resources as mean temperatures are increasing, rainfall

regime is shifting from temperate to tropical characteristics in the middle latitudes (Sabattini and Sabattini 2021) and sea level is rising with an accelerating rate in the coming decades (IPCC 2023). The sea level change will increase the seawater head at the coast with the consequent migration of the freshwater–seawater interface inland (Ketabchi et al. 2016). These factors will intensify seawater contamination, reduce the groundwater table and enhance the negative effects on crop production and freshwater storage (Manoli et al. 2006; Samadder, Kumar, and Gupta 2011). In addition, sea level rise also is going to increase coastal erosion resulting in shoreline retreat and reduction of the areas where groundwater is stored (Oude Essink 2001). The negative effects of sea level rise are expected to have a greater impact on the saltwater plume progression in the areas where the groundwater head is artificially controlled by drainage systems (Rasmussen et al. 2013). This condition is typical of the low-lying reclaimed farmlands near the Venice Lagoon, Italy, where the water table is maintained at a suitable depth for farming by networks of ditches and pumping stations (Da Lio et al. 2015; Tosi et al. 2022).

In coastal regions, SWI may be also enhanced by the presence of highly permeable paleochannels. These features are made of highly permeable coarse sediments and provide a hydraulic connection between the aquifers and the sea (Falls et al. 2005). The role of paleochannels in groundwater-seawater exchanges was extensively studied by Mulligan, Evans, and Lizarralde (2007) through numerical modelling demonstrating that these coarse structures increase both seawater water inflow and freshwater outflow.

Before implementing technical interventions, the control of SWI requires the monitoring and modelling of groundwater-seawater dynamics to develop a mitigation plan. Among the possible countermeasures against SWI in coastal areas, the most effective are (i) freshwater recharge through coastal artificial wells, (ii) reduction of freshwater extraction and (iii) installation of physical barriers (Oude Essink 2001; Hussain et al. 2019). Recently, Motallebian et al. (2019) proposed an innovative approach that consists of a freshwater recharge using the water of a surface artificial channel that flows to the aquifer by hydraulic gradient (i.e., the water level in the stream is higher than the water level in the aquifer). Despite the huge initial work for the construction of the hydraulic control structure, this method is easily manageable in the long term. Their modelling results demonstrated that the implementation of a surface water recharge channel is effective in reducing the saltwater wedge.

In the low-lying farmlands along the Venice coastland, Italy, SWI is a widespread phenomenon exacerbated by the presence of sandy paleochannels, land subsidence, seawater encroachment along the main watercourses, and peat-driven salinity that cause the seawater plume to extend up to 20 km inland (Carbognin et al. 2010; Da Lio et al. 2015; Zancanaro et al. 2020; Alessandrino et al. 2023). In this context, the research project MoST/SeCure funded by the EU within the Interreg IT-CR Programme has been recently conducted to characterise the origin of the salt contamination and suggest possible mitigation and adaptation strategies. This study introduces the results of a new technique to mitigate SWI, involving the controlled discharge of freshwater through a 200 m-long buried drainpipe positioned along a well-preserved sandy paleochannel. The infrastructure was installed in an agricultural experimental field located at the southern margin of the Venice Lagoon in the fall of 2020. A monitoring network was established to assess the drainpipe effects on soil and groundwater quality operating 2 years before and 2 years after drainpipe installation. The unique datasets acquired over the 2019–2022 monitoring period are presented and analysed. The records allow to build up a clear picture of the tested countermeasure effectiveness.

2 | Materials and Methods

2.1 | The Study Area

The study area is located on the southern margin of the Venice Lagoon, Italy (45°10′57″ N, 12°13′55″ E) and is bounded to the north by the Brenta and Bacchiglione rivers and the Morto reclamation channel (Figure 1). The area lies below the mean sea level (msl) with elevations ranging from −1.5 to −3.3 m. The actual altimetric variability is mainly derived from the different elevations of ancient swamps, paleochannels and littoral ridges characterising the area before land reclamation occurred

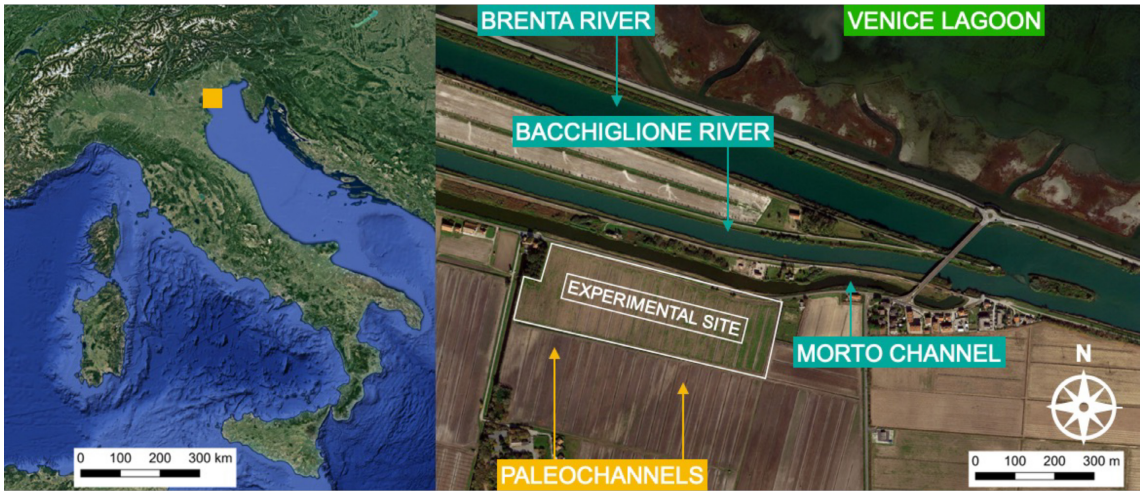

FIGURE 1 | Location of the experimental site, the main watercourses, the Venice lagoon and the main sandy paleochannels.

between 1892 and 1967 (Cavallina et al. 2022). The water table is artificially controlled by a network of ditches and a pumping station that brings the excess water from the agricultural area to the lagoon. The upper 1 m soil is mainly silty clay (Molli-Gleyic Cambi-sols, FAO-UNESCO. 1989) with peat deposits and a coarse well-preserved paleochannel that crosses the experimental area in a southwest to northeast direction.

The experimental site (Figure 1) is an 11-ha field that was cultivated with rainfed maize in 2019 (planting date 3/24, harvest date 10/1), 2020 (planting date 3/23, harvest date 9/11), 2021 (planting date 3/25, harvest date 9/10) and 2022 (planting date 4/5, harvest date 9/3).

2.2 | The Experimental Infrastructure

The experimental infrastructure (Figure 2) was established in the fall of 2020, tested for the first time from 8/2/2021 to 9/7/2021 and became fully operational in 2022, from 6/16 to 8/24. The infrastructure consisted of an intake (Figure 2b) from the Morto channel, through a vertical pipe with two openings located at different heights and a control valve for each opening. It supplied freshwater by gravity into a 200 m-long buried pipe drain with a diameter of 0.16 m. The corrugated polyethylene drainpipe was installed at 1.5 m depth along the 10 to 15 m-wide eastern paleochannel by digging a 0.5 m-wide trench (Figure 2a). The whole system of pipes and valves was placed inside a concrete structure supported by a foundation made of wooden logs. A maximum 2.25 m head difference between the water level in the Morto channel and the water table in the surrounding farmland guaranteed a maximum discharge rate of 28 $L\,s^{-1}$.

The actual water flux, as measured by a flowmeter (3070, KROHNE Messtechnik GmbH, Duisburg, Germany) was controlled by two valves, one located upstream and the other downstream. The flow rate was manually recorded during the 2021 recharge test and automatically, every 10 min, in 2022, by connecting the flowmeter to a SOFREL datalogger (LACROIX Sofrel, Vern-sur-Seiche, Rennes, France) (DR, Figure 3a). A bentonite cut-off wall (Figure 3a) was realised at the southern extremity of the drainpipe to reduce the freshwater dispersion

FIGURE 2 | Pictures of the experimental infrastructure: The drainpipe path along the experimental field after the trench digging and the corrugated polyethylene drainpipe establishment (a), the intake (b) and the excavation after soil piping occurred in preliminary tests carried out in 2020 (c).

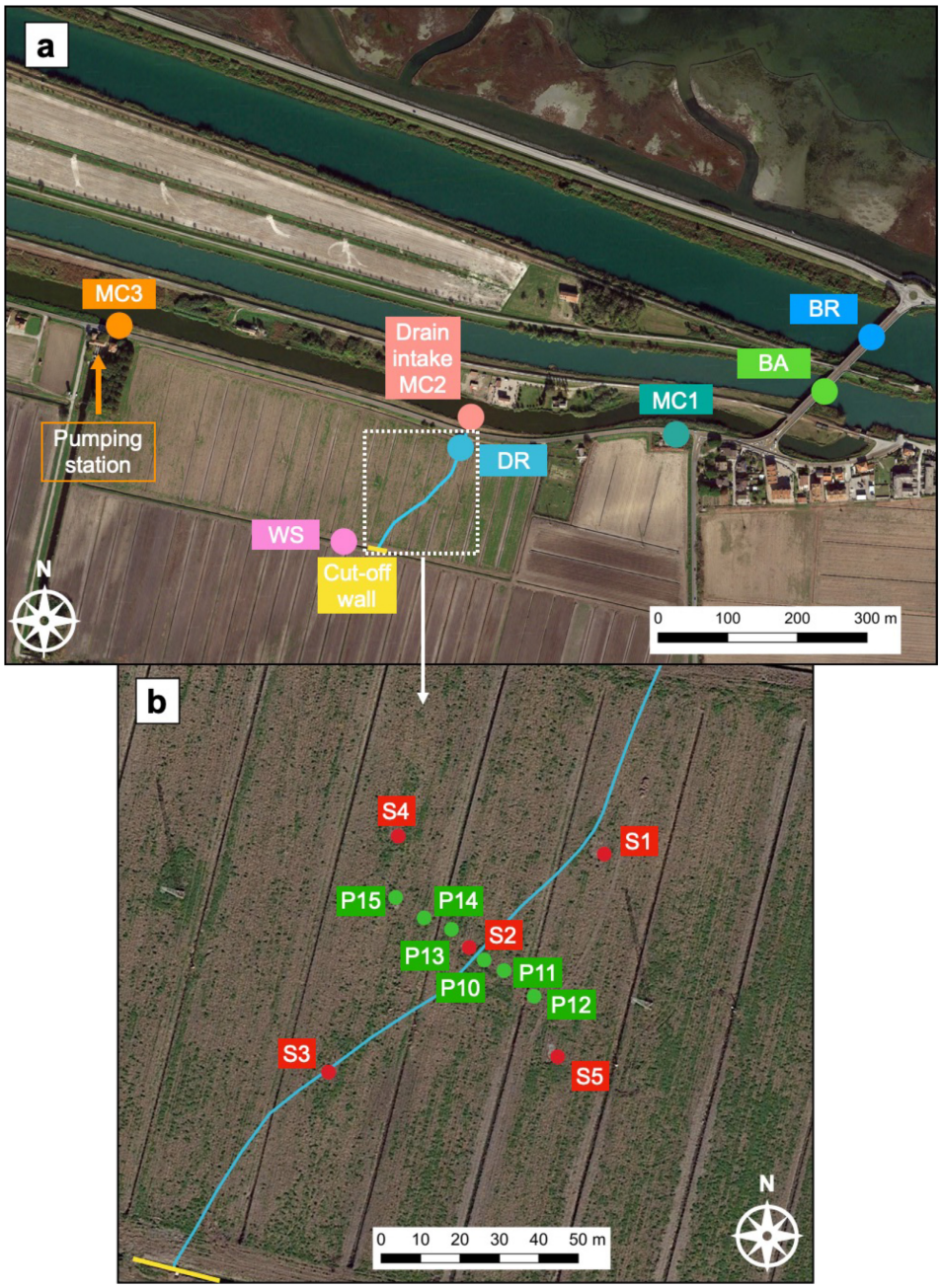

FIGURE 3 | The experimental area with (a) the location of the monitoring sites on Brenta river (BR), Bacchiglione river (BA) and Morto Channel (MC1, MC2 and MC3), the drainpipe path, the flowmeter (DR), the cut-off wall and the weather station (WS); (b) zoom in the drainpipe area with the location of the monitoring sites in the experimental field.

associated with the north-to-south natural groundwater flow regime.

Furthermore, in 2021 the electrical conductivity (EC_w) of the recharge water was manually monitored with a four-electrode-conductivity cell equipped with a built-in temperature sensor (TetraCon 325, WTW, 2021 Xylem Analytics Germany Sales GmbH & Co. KG). However, for the 2022 season, a EC_w meter (ST 3254.1, Royce Water Technologies Pty Ltd., QLD, Australia) was installed at the intake (MC2, Figure 3a) to facilitate continuous monitoring. This was achieved through a SOFREL datalogger (LACROIX Sofrel, Vern-sur-Seiche, Rennes, France) recording the Morto channel EC_w every 10 min.

2.3 | Boundary Conditions: Morto Channel, Rivers and Weather Data

The EC_w vertical profile in the Brenta river, Bacchiglione river and Morto channel was manually acquired at the locations BR, BA, MC1 and MC3, respectively (Figure 3a) with a four-electrode-conductivity cell with a built-in temperature sensor (TetraCon 325, WTW, 2021 Xylem Analytics Germany Sales GmbH & Co. KG). The Morto Channel EC_w was measured at two depths (top and bottom), while the EC_w of Brenta and Bacchiglione rivers was measured at various levels, including the top, bottom and 1-m intervals from the top to the bottom.

Weather hourly data (rainfall, solar radiation, temperature, relative humidity, wind speed and direction) were measured and recorded with an on-site ATMOS 41 all-in-one weather station (METER Group, Inc., Pullman, WA, USA) connected to a ZL6 datalogger (METER Group, Inc., Pullman, WA, USA) (WS location, Figure 3a). The reference evapotranspiration (ET_0), that is, the evapotranspiration from a standardised vegetated surface, was computed according to the Penman-Monteith equation. Considering that the experimental site was cultivated with maize, the crop type, variety and development stage were considered by calculating the crop evapotranspiration following the FAO56 single crop coefficient (K_c) approach described by Allen et al. (1998) and obtaining the evapotranspiration under standard conditions (ET_c). The K_c varied during the growing season according to the maize phenological stage. Then, the effective evapotranspiration (ET_e) was obtained by multiplying the ET_c by the water stress coefficient (K_s) that describes the effect of water stress on crop transpiration. K_s was calculated according to Allen et al. (1998) and considering a depletion factor of 0.5.

2.4 | Monitoring Network

The monitoring network was established between planting and harvest, according to field operations, in 2019 (from 7/21 to 1/20), 2020 (from 5/30 to 11/11), 2021 (from 6/8 to 10/28) and 2022 (from 6/7 to 10/5). Five monitoring sites (S1, S2, S3, S4 and S5; Figure 3b) were installed and equipped with:

- a 2.5 m deep piezometer to monitor depth to the water table and groundwater EC_w (mS cm^{-1});
- four TEROS-12 soil moisture (WC, m^3 m^{-3}), bulk electrical conductivity (EC_b, mS cm^{-1}) and temperature (°C) sensors (METER Group, Inc., Pullman, WA, USA) at four depths (0.1, 0.3, 0.5 and 0.7 m). The EC_b measured by TEROS-12 sensors was converted to pore electrical conductivity (EC_p, mS cm^{-1}) according to the Hilhorst (2000) equation. Hourly data were recorded by ZL6 dataloggers (METER Group, Inc., Pullman, WA, USA).

Three stations were placed along the paleochannel (S1, S2 and S3), while S4 and S5 were placed about 30 m outside (Figure 3b). Moreover, in 2021 and 2022 six additional 2.5 m deep piezometers were installed at a distance of 5, 10 and 20 m from both sides of S2 to monitor the lateral spread of freshwater supplied by the drainpipe (Figures 3b and 4). Depth to the water table and groundwater EC_w were measured weekly with a portable water level meter and a four-electrode-conductivity cell with a built-in temperature sensor (TetraCon 325, WTW, 2021 Xylem Analytics Germany Sales GmbH & Co. KG), respectively.

2.4.1 | Electrical Resistivity Tomography

In 2021 and 2022, sites S1 and S2 were also equipped with electrical resistivity tomography (ERT) lines crossing the recharging drainpipe through a timelapse approach (TL-ERT) (Figure 4). Surveys were collected using a Syscal Junior 72 resistivimeter (Iris Instruments, Orleans, France) with a dipole–dipole skip 0 array on a transect line of 14.1 m composed of 48 stainless-steel electrodes spaced 0.3 m, reaching an investigation depth around 2.5 m. Along each line, 2195 quadrupoles were acquired, with a stacking quality factor 'Q' set to 1% (3 to 6 stacks) and adopting a current injection time of 250 ms per cycle. Datasets were pre-processed to remove unreliable data, and a model based on the reciprocal errors was used to estimate the data errors. Surveys from 2021 monitoring were analysed in terms of direct-reciprocal deviation with a 5% threshold (Binley, Ramirez, and Daily 1995), and cleaned from apparent resistivities ρ_a outside the range 2–50 Ωm, while for 2022 data the threshold for reciprocals was 8% and the ρ_a range of 4–80 Ωm. The inversion process, that is, the transformation of the acquired resistivity data into a subsurface resistivity model, was performed by adopting the respective error threshold, plus a 3% which considers the systematic error, with the open-source C++/Python-based library pyGIMLi (Rücker, Günther, and Wagner 2017). PyGIMLi utilises a finite element approach, discretizing the subsoil model with the same unstructured triangular mesh, and allows the choice of regularisation and smoothing parameters to be used in the inversion process (Wagner and Uhlemann 2021).

Acquisitions were performed on five dates in 2021, two before (7/2/2021 and 7/30/2021) and three after the drain opening (8/10/2021, 8/20/2021 and 9/7/2021), while four acquisitions were performed in 2022, one before (6/10/2022) and three after the drain opening (7/4/2022, 7/21/2022 and 8/4/2022). The novel four-dimensional (4-D) inversion technique, firstly proposed by Kim et al. (2009), was used to process the time lapse surveys. In this approach, the data from all time-steps in the sequence are inverted simultaneously with smoothness constraints applied in both the spatial and temporal dimensions. Where the data pre-processing removed measurements, the missing quadrupoles were assigned a median resistivity value and down-weighted in the inversions, as described in

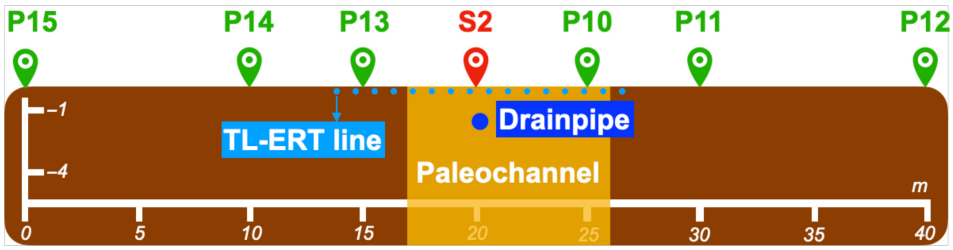

FIGURE 4 | Vertical section of the experimental field highlighting the position of S2 and its TL-ERT line, P locations, the drainpipe and the paleochannel extent.

Wilkinson et al. (2022). In this way, resistivity changes (difference %) over time were obtained reducing the noise propagation within the modelled timesteps, which usually generate false anomalies of soil condition changes.

2.5 | Soil and Groundwater Sampling

Disturbed soil samples were collected at four depth intervals (i.e., 0 to 0.2 m, 0.2 to 0.4 m, 0.4 to 0.6 m and 0.6 to 0.8 m) per each monitoring location and analysed for granulometry (sand, silt and clay fractions) trough laser diffraction method (Mastersizer 2000, Malvern Panalytical Ltd., UK) and converted into pipette one (Bittelli et al. 2019). Moreover, S locations were also analysed for soil organic carbon (SOC, %), electrical conductivity (EC_e 1:5, mS cm^{-1}), pH and cation exchange capacity (CEC meq 100 g^{-1}). Moreover, undisturbed soil cores were collected at the four depths with a hydraulic sampler to perform the hydraulic characterisation of the upper 0.8 m vadose zone. Saturated hydraulic conductivity (K_s) was measured on 0.08 m diameter and 0.05 m height cores using a laboratory permeameter (Eijkelkamp, Giesbeek, The Netherlands). Retention curves were determined on 0.05 m diameter and 0.025 cm height cores by applying the Sandbox method (Eijkelkamp, Giesbeek, The Netherlands) and a 5-bar pressure plate extractor (Soilmoisture Equipment Corp., Santa Barbara, CA, USA). Samples were then oven-dried at 105°C for 24 h to calculate bulk densities (BD, g cm^{-3}) according to the core method (Grossman and Reinsch 2002).

Groundwater samples were monthly collected at each piezometer during the crop seasons from 2019 to 2022. Samples were stored at 4°C and analysed at the end of each monitoring to determine EC_w (mS cm^{-1}), pH and Cl^-, Br^-, NO^{3-}, PO_4^{3-}, SO_4^{2-}, Na^+, K^+, Mg^{2+}, Ca^{2+} ionic concentrations (mg L^{-1}). All the analyses refer to a standard temperature of 25°C.

2.6 | Data Analysis

Possible relationships between groundwater, soil water, SWI and boundary conditions were investigated with three methods:

a. Univariate simple statistics. Groundwater variables were tested with non-parametric methods since data showed a non-normal distribution. Univariate simple statistics were applied to each chemical parameter and EC_w was plotted against the most abundant ions in seawater (i.e., Cl^-, Na^+ and SO_4^{2-}) using Spearman's rank correlation coefficients (Millero et al. 2008; Werner et al. 2013).

b. Principal component analysis (PCA). The PCA technique (Greenacre et al. 2022) was applied to investigate possible relationships between boundary conditions, groundwater and soil water data. Three PCAs were performed: 2019–2020 (i.e., the period before the freshwater recharge), 2021 and 2022. The investigated variables are: rain, ET_e, EC_w measured at MC1, EC_w measured at MC3, drain flow rate (for 2021 and 2022 only), recharge water EC_w (for 2022 only), soil water content as function of the readily available water (WC_a) to account for the different soil hydraulic properties among the monitoring sites, EC_p, groundwater EC_w, major groundwater ions (Cl^-, Br^-, SO_4^{2-}, Na^+, K^+, Mg^{2+}, Ca^{2+}), Cl/Br ratio and depth to the water table. The significance of the eigenvalues was demonstrated by the Bartlett Test (Bartlett 1951).

c. Cl/Br molar ratios calculation. Cl^- and Br^- are conservative tracers and their ratio remains constant even if their concentrations change due to physical processes. The effectiveness of the Cl/Br ratio in the identification of groundwater salinity origin was well documented in Alcalá and Custodio (2008) and Zancanaro et al. (2020).

3 | Results

3.1 | Soil Properties

The results of soil analyses are summarised in Table 1 by averaging the depth 0.4–0.6 with 0.6–0.8 as the layers were considered homogeneous.

The three stations located on the paleochannel were characterised by sandy loam to loamy sand soil with an increase in sand content and BD in a southwesterly direction (i.e., from S1 to S3). $EC_e < 0.4$ mS cm^{-1} was found at S2 and S3, while S1 (i.e., the closest to rivers and lagoon) was characterised by a higher EC_e and CEC compared to S2 and S3. The soil layer 0.4–0.8 m on both sides of S2 was sandy loam, except for P13 which was loam at all depths.

S4 and S5 are located outside the paleochannel and are both characterised by a peat layer between 0.4 and 0.6 m deep at S4 (BD = 0.36 g cm^{-3}) and between 0.4 and 0.8 m deep at S5 (BD = 0.23 g cm^{-3} at 0.4–0.6 m and 0.21 0.36 g cm^{-3} at 0.6–0.8 m). The peat layers were also characterised by higher EC_e compared to the top 0–0.4 m layer with S5 being the most saline monitoring location.

3.2 | Hydrologic Boundary Conditions

3.2.1 | Weather

Variable meteorological conditions were observed during the 4-year study (Figure 5). In fact, 2019 was characterised by intense rainfall for the whole cropping season with a total of 524 mm from April to September, except for June when temperatures were 24.7°C on average and rainfall was 2 mm. Differently, the 2020, 2021 and 2022 cropping seasons were characterised by similar cumulative rainfall (249, 227 and 264 mm between April and September, respectively). The 2022 season was the driest one because of the exceptionally scarce rainfall and high temperatures recorded from June to August. The severe conditions had profound effects on the productivity of the entire agricultural area.

3.2.2 | Surficial Water Salinity

Seawater encroachment along the Bacchiglione and Brenta rivers varied according to monitoring dates and depths (Figures 6 and 7). As the monitoring locations (Figure 3a) were close to the river mouth (approximately 6 km), saltwater was commonly observed in

TABLE 1 | Soil texture (sand, silt and clay %), bulk density (BD), soil organic carbon (SOC), soil water extract EC (EC_e), pH and cation exchange capacity (CEC) characterising the depths 0–0.2, 0.2–0.4 and 0.4–0.8 m at the monitoring locations.

Monitoring location	Depth (m)	Sand 2000–50 μm (%)	Silt 2–50 μm (%)	Clay <2 μm (%)	BD (g cm^{-3})	SOC (%)	EC_e 1:5 (mS cm^{-1})	pH1:2	CEC (meq $100\,g^{-1}$)
S1	0–0.4	28.76	56.12	15.12	1.11	8.15	0.40	7.70	75.06
	0.4–0.8	54.21	35.64	10.15	1.16	8.85	1.19	7.38	61.30
S2	0–0.4	31.10	52.77	16.13	1.26	5.70	0.37	7.55	50.97
	0.4–0.8	69.93	21.15	8.92	1.52	4.91	0.29	8.03	50.51
S3	0–0.4	33.16	50.94	15.90	1.10	6.80	0.37	7.59	55.05
	0.4–0.8	77.19	15.73	7.08	1.42	6.76	0.29	7.99	51.13
S4	0–0.4	21.26	59.49	19.25	1.17	6.53	0.41	7.86	59.43
	0.4–0.8	51.68	37.43	10.89	0.70	6.51	0.83	7.84	58.15
S5	0–0.4	29.77	53.25	16.98	0.99	9.88	0.45	7.57	78.37
	0.4–0.8	72.09	21.79	6.12	0.11	10.35	2.13	5.96	76.57
P10	0–0.4	34.16	50.33	15.51	—	—	—	—	—
	0.4–0.8	72.79	19.36	7.84	—	—	—	—	—
P11	0–0.4	30.28	53.55	16.17	—	—	—	—	—
	0.4–0.8	65.05	27.51	7.44	—	—	—	—	—
P12	0–0.4	34.04	50.19	15.77	—	—	—	—	—
	0.4–0.8	59.93	29.83	10.24	—	—	—	—	—
P13	0–0.4	30.60	53.75	15.65	—	—	—	—	—
	0.4–0.8	55.83	33.46	10.71	—	—	—	—	—
P14	0–0.4	38.17	48.28	13.55	—	—	—	—	—
	0.4–0.8	45.48	43.06	11.45	—	—	—	—	—
P15	0–0.4	25.14	52.27	17.60	—	—	—	—	—
	0.4–0.8	53.95	37.12	8.93	—	—	—	—	—

the deeper part of the water column, particularly during high-tide conditions and in the absence of significant rainfall events on the river catchments. In these situations, the river discharge may only partially counteract the encroachment of seawater from the river mouth. In 2019, 2020 and 2021 the top 2 m of the water column were predominantly fresh, but in 2022 there was a notable worsening of SWI, leading to the salinization of the whole water profile. Brenta was saltier than Bacchiglione in 2019, 2020 and 2021 with median bottom EC_w values equal to 42.6 versus 14.9 mS cm^{-1} in 2019, 39.9 versus 11.98 mS cm^{-1} in 2020, 48.1 versus 19.12 mS cm^{-1} in 2021. Similar values were recorded in 2022 (49.4 versus 51.5 mS cm^{-1}, respectively). Notice that the proximity to the sea restricts substantial fluctuations in water levels in the two watercourses.

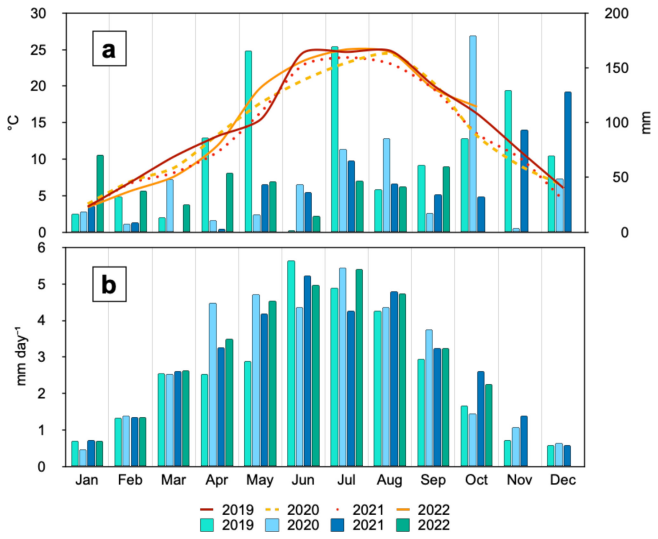

FIGURE 5 | (a) Averaged daily temperature and cumulative monthly rainfall, and (b) averaged monthly ET_0 in 2019, 2020, 2021 and 2022. Mean temperatures are represented by lines, while cumulative rainfall and mean ET_0 are represented by bars.

The Morto channel was monitored at MC1 and MC3 locations (Figure 3a). This artificial channel, collecting water from the nearby farmland, is fresher than the Brenta and Bacchiglione rivers (Figure 8). Except for 2019, the median yearly EC_w was always lower than 3.5 mS cm^{-1}. The lowest salinity and the smallest vertical fluctuation over time were recorded at MC1. The saltier inflow of the pumping station adduction channel negatively affected MC3. The top water was always (almost) fresh with median values of 0.9, 1.4, 1.2 and 2.0 mS cm^{-1} in 2019, 2020, 2021 and 2022, respectively. The water level of the channel is kept constant, with fluctuations limited to around 0.1 m.

3.3 | Groundwater and Soil Conditions in 2019 and 2020, Before the Freshwater Recharge

The mean water table decreased along the main paleochannel in the southwestern direction (i.e., from S1 to S3) during both 2019 and 2020 (Figure 9). The shallowest water table was observed at S5 with an average depth to the water table equal to 0.5 in 2019 and 0.6 m in 2020, respectively.

Groundwater was mildly brackish along the main paleochannel, with a slight EC_w increase from the location closer to the Morto channel to the southwest direction (i.e., from S1 to S3, Figure 10a). The median EC_w values were 2.7 mS cm^{-1} at S1, 3.1 mS cm^{-1} at S2 and 3.9 mS cm^{-1} at S3 in 2019, while 3.1 mS cm^{-1}, 3.2 mS cm^{-1}

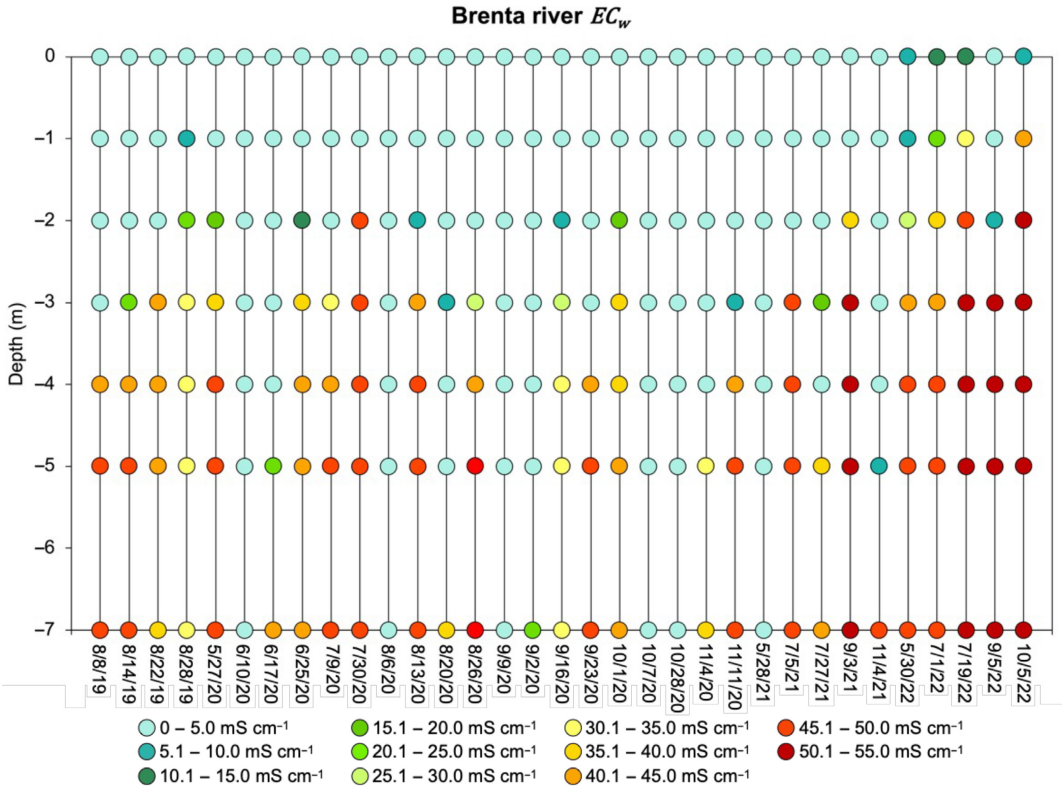

FIGURE 6 | EC_w vertical profiles recorded in the Brenta river during the monitoring period.

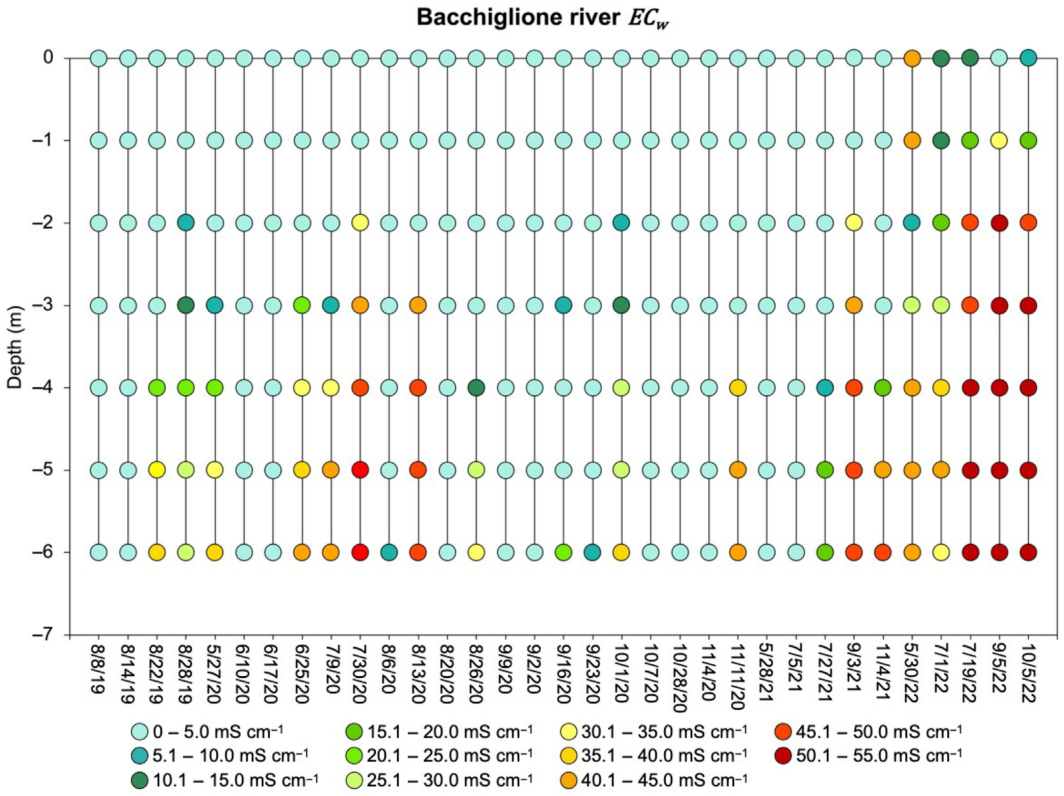

FIGURE 7 | EC_w vertical profiles recorded in the Bacchiglione river during the monitoring period.

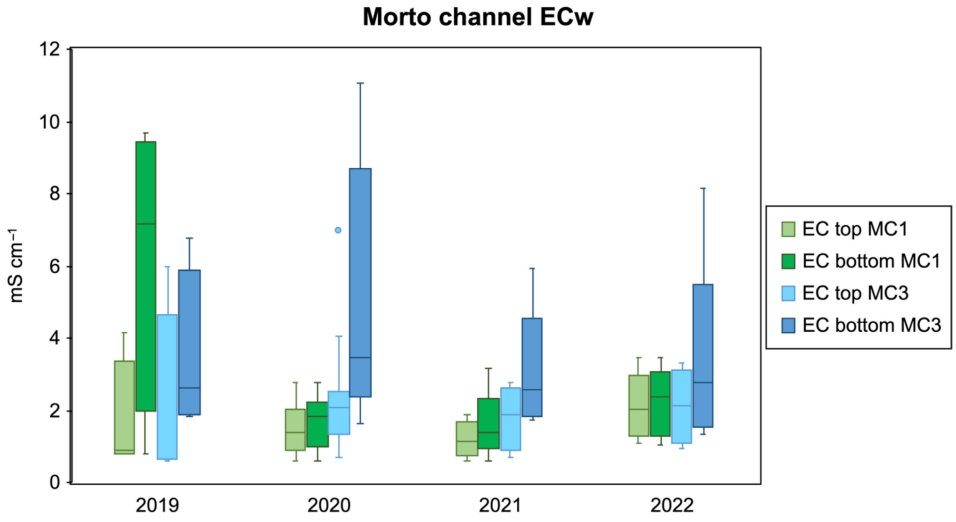

FIGURE 8 | Box plot of Morto channel top and bottom EC_w measured at locations MC1 and MC3 during the 4-year study. Outliers are plotted as individual points.

and 3.4 mS cm^{-1} in 2020, respectively. Cl/Br molar ratio close to seawater value was measured at S1 while the molar ratio decreased with the distance from the seawater sources (i.e., rivers and lagoon, Figure 10b). The two monitoring sites outside the paleochannel showed an opposite behaviour: groundwater at S4 was almost fresh with negligible EC_w variability among dates and Cl/Br lower than seawater value, while S5 was saline (EC_w medians 6.54 and 4.56 mS cm^{-1} in 2019 and 2020, respectively) with Cl/Br equal or higher than seawater value.

Significant correlations were found between groundwater EC_w, Cl^- and Na^+ concentrations in both 2019 ($p = 0.0002$ and $p = 0.0001$, respectively) and 2020 ($p < 0.0001$). No dependency was found between EC_w and SO_4^{2-} (Table 2).

3.4 | Groundwater and Soil Conditions in 2021 and 2022 During the Freshwater Recharge

3.4.1 | Drain Flow Rate and Input Water EC_w

The 2021 freshwater recharge started on 2 August 2021, with a flow rate of 9 $m^3 h^{-1}$, then decreased to 3.3 $m^3 h^{-1}$ on 11 August 2021, and was kept almost constant until 7 September 2021,

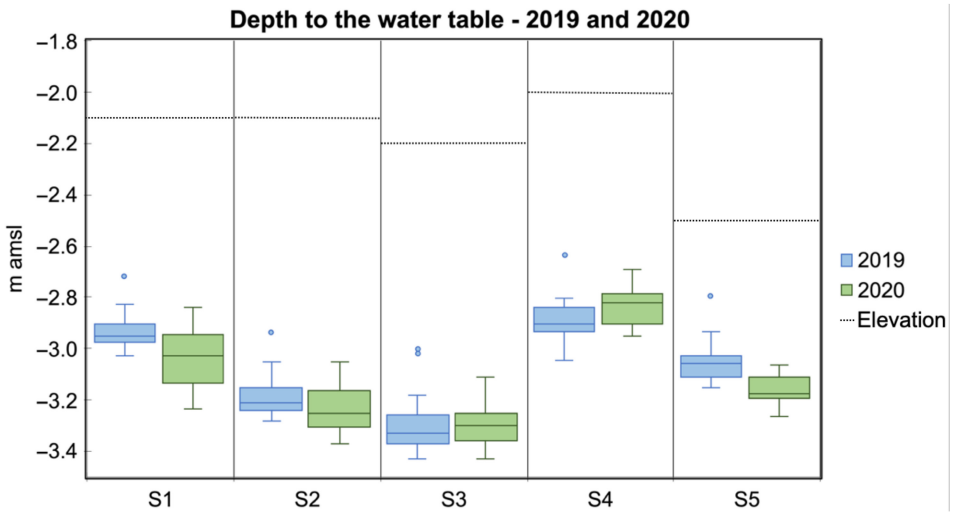

FIGURE 9 | Land elevation and mean elevation of the water table (amsl) measured in 2019 and 2020 at the five monitoring stations.

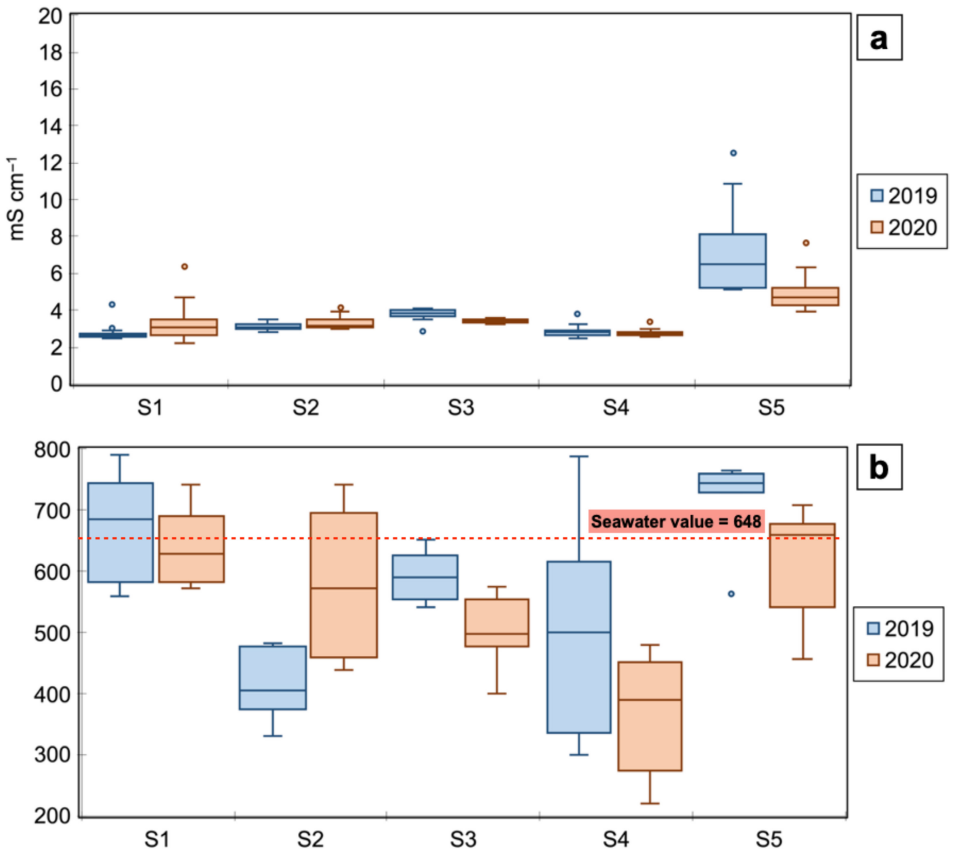

FIGURE 10 | Box plot of groundwater EC_w (a) and Cl/Br molar ratio (b) measured in 2019 and 2020.

that is a few days before maize harvesting (Figure 11a). The discharge values were reduced with respect to the potential maximum value to avoid soil piping as occurred in preliminary tests carried out in 2020 (Figure 2c). The input water EC_w was 2.2 mS cm^{-1} on average.

The freshwater recharge in 2022 started on 16 June and ended 1 week before maize harvesting on 24 August. The drain flow rate was highly variable, averaging 8.8 $m^3 h^{-1}$ (DR, Figure 3a). The operations were halted on 6/20/2022 and again from 6/28/2022 to 7/3/2022 due to vegetal residues that clogged the deepest opening of the intake infrastructure. The drain flow rate varied also in response to fluctuations in the water level in the Morto channel. The input water EC_w varied between 0.5 to 7.5 mS cm^{-1} (Figure 11b), exceeding the values recorded in 2021. This increase can be attributed to the severely dry season, restricting the conveyance of freshwater toward the coastal zone. This is also confirmed by the manual measurements on the locations MC1 and MC3 (Figure 3a).

3.4.2 | Groundwater Monitoring

The mean depth to the water table was similar in 2021 and 2022. For example, the mean values are 1.0 and 0.9 m below the soil surface (bss) at S1, 1.13 m bss in both years at S3 and 0.6 m bss in both years at S5. In 2021, following a period of negligible variations, the water table experienced a steady rise of approximately 0.1 to 0.2 m during the recharge phase. Upon closure of the drain, the water table gradually returned to its original lower elevation over about 2 months (Figure 12a). The trends in 2022 were more complex, with the water table initially deepening during the first 2 weeks of recharge, consistent with the observed trend before the drainpipe opening. Subsequently, with the infiltration of larger discharge rates (Figure 11), the water table began to rise, resulting in an elevation gain of about 0.05 to 0.1 m at the end of the recharging phase, after which the levels stabilised. These effects were more pronounced in S1 and less noticeable in S5 during both monitored years (Figure 12b).

Groundwater EC_w remained consistently higher in 2021 and 2022 compared to the previous 2 years, especially at S1, S3 and S5 (Figures 10a and 13a). For example, the medians EC_w at S1 were 15.6 and 10.2 mS cm^{-1} in 2021 and 2022, respectively. Except for P15, Cl/Br molar ratio was almost equal to the seawater value at all monitoring locations in 2021. An evident decrease in groundwater EC_w of about 75% between the opening and closing dates of freshwater recharge was observed at S1, that is the site closer to the intake (Figure 14a). Freshening was negligible in S2 and S3. A EC_w reduction of 30% was also observed at P11, while an initial decrease followed by an EC_w rise was observed at P12, P14 and S5.

Although the EC_w measured in 2022 confirms the groundwater salinization also detected in 2021, Cl/Br molar ratio reflected a freshening process at S2, S4, P10, P11, P12, P13 and P14 in 2022 (Figure 13b). A reduction of groundwater EC_w was observed at S1 (36%) and S3 (14%) during the freshwater recharge. An initial EC_w reduction followed by an increase was observed at S2, S4, S5, P11, P12 and P14 (Figure 14b).

Significant positive correlations were found between groundwater EC_w and the major seawater ions (i.e., Cl^-, Na^+ and SO_4^{2-}; Table 3). The relationships were stronger between EC_w, Cl^- and Na^+ ($\rho = 0.92$ and 0.88, respectively, with $p < 0.0001$) than between EC_w and SO_4^{2-} ($\rho = 0.58$, with $p = 0.03$ and $p < 0.0001$ in 2021 and 2022, respectively).

TABLE 2 | Spearman's correlations (ρ) between groundwater EC_w (mS cm^{-1}) and Cl^-, SO_4^-, Na^+ (mg L^{-1}) ion concentrations measured in 2019 (blue cells) and 2020 (green cells).

	ECw	Cl^-	SO_4^{2-}	Na^+
ECw	1.00	**0.63**	0.21	**0.67**
Cl^-	**0.74**	1.00	−0.22	**0.92**
SO_4^{2-}	−0.02	**−0.51**	1.00	−0.14
Na^+	**0.81**	**0.95**	**−0.44**	1.00

Note: Values range from −1 to +1 with larger absolute values indicating a stronger relationship. Bold values indicate a significant correlation ($\alpha = 0.05$).

3.4.3 | Soil Water: EC_p and WC

Figures 15 and 16 depicted WC and EC_p recorded in 2021 and 2022 at sites S1 and S3 located inside the paleochannel and site S5 located outside the paleo-river bed. The charts of WC and EC_p at S2 and S4 are available in the Supporting Information.

WC values increased during the rainfall events, particularly at 0.1 and 0.3 depths. The highest WC was observed in the peaty layers at S5 in both 2021 and 2022 (Figure 15c,f), while S3 was

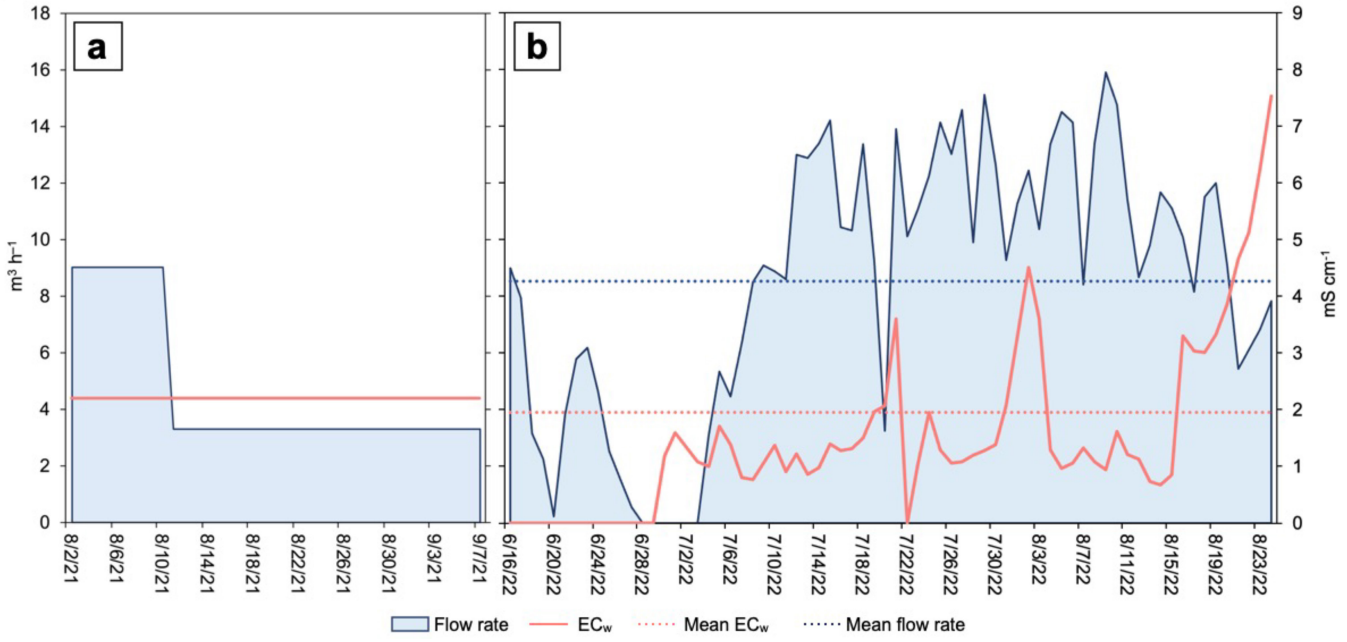

FIGURE 11 | Drainpipe flow rate and input water EC_w measured at the drainpipe intake (MC2) during the 2021 (a) and the 2022 (b) cropping seasons.

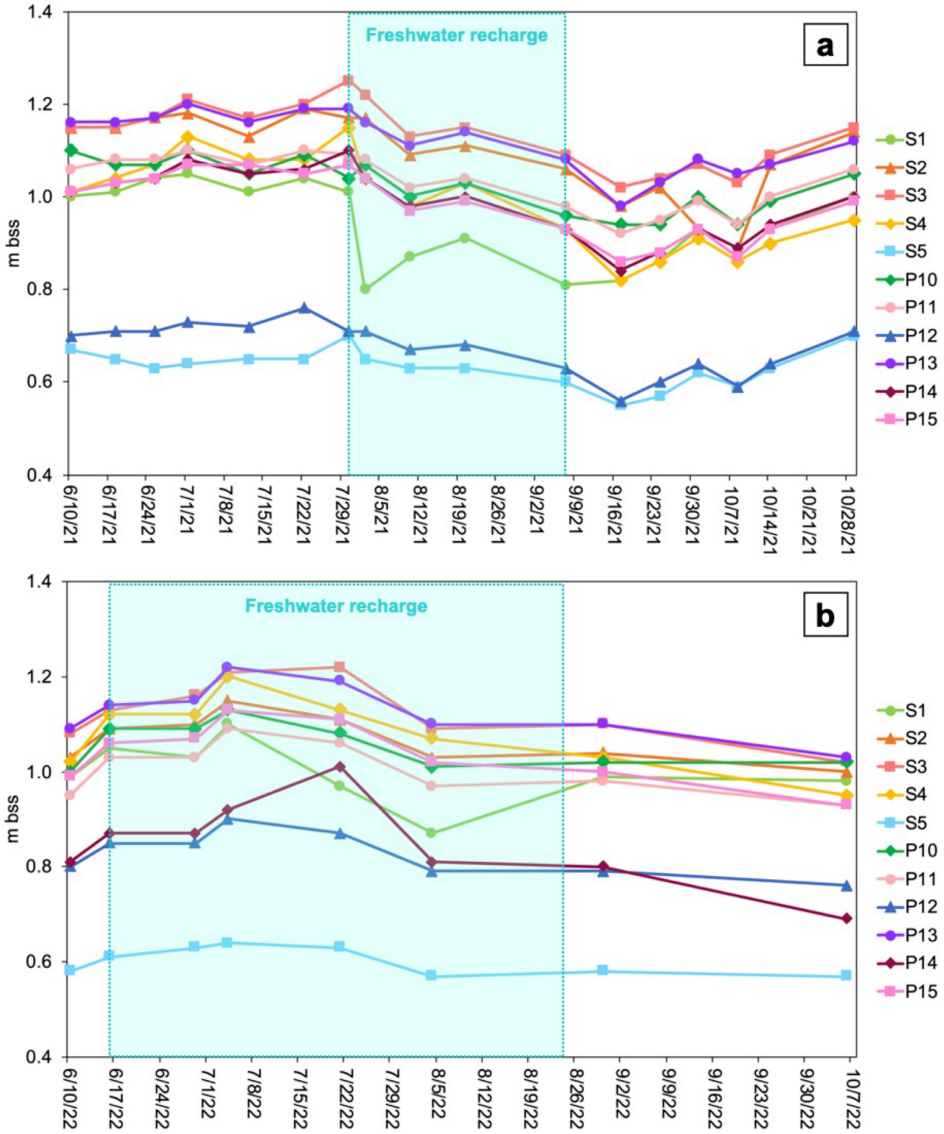

FIGURE 12 | Depth to the water table measured in 2021 (a) and 2022 (b).

the driest monitoring location (Figure 15b,e). Looking at the bottom layers at S1 and S3, the dataset does not show significant increases in WC during the freshwater recharge tests except for the 0.3 m sensor of S1 in 2022 (Figure 15d).

Similarly, as observed in the results for WC, EC_p was highly sensitive to rainfall events, leading to an increase in pore water salinity, especially in the upper layers. The EC_p did not decrease during the freshwater recharge tests either in 2021 or 2022. On the contrary, an increase of EC_p was observed at 0.5 m depth in S1 (Figure 16a) and 0.3 and 0.7 m depths in S3 (Figure 16b,e).

3.4.4 | Time-Lapse Electrical Resistivity Tomography (TL-ERT)

The outcomes of the TL-ERT acquisitions performed during the 2021 recharge test, comprising three prior to its beginning and three after, are reported in Figure 17. In general, the range of resistivity found is 0–50 Ωm and the initial models show a continuous horizontal stratification, with a more resistive top layer (> 35 Ωm) and decreasing values at depth (< 15 Ωm). The results are presented in terms of resistivity change (in percentage) relative to the first acquisition. An increase in soil resistivity is observed after the beginning of the freshwater recharge test at both monitoring sites S1 and S2. At S1 (the site closer to the drain intake, Figure 3), the increase of resistivity around the drainpipe was already evident on 8/10/2021. The freshwater lens gradually spread both laterally and vertically until the end of the recharge phase, when the resistivity increase was > 50% (i.e., the resistivity was ~5.0 Ωm on 7/30/2021 and ~15.0 Ωm on 9/7/2021). A similar pattern is noted at S2, although the soil resistivity increase was clear only after 8/20/2021 and the lateral spread of the freshwater lens was lower. However, the resistivity increase was >50%, with an initial value of ~5.0 Ωm on 7/30/2021 and 25.0 Ωm on 9/7/2021 (Figure 17).

TL-ERT acquisitions were also performed in 2022, one before the freshwater recharge test (i.e., on 6/10/2022) and three during the recharge operation. The outcomes showing the incremental

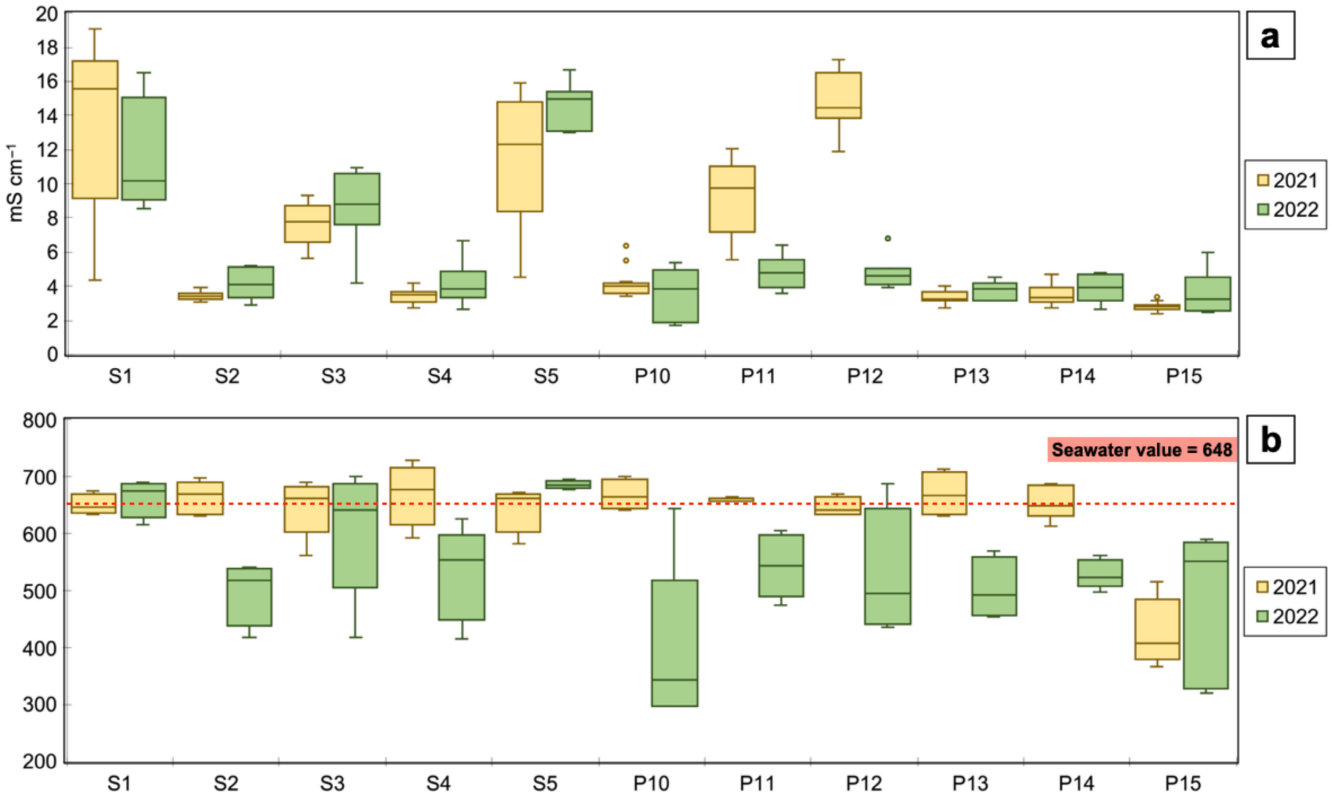

FIGURE 13 | Box plot of groundwater EC_w (a) and Cl/Br molar ratio (b) measured in 2021 and 2022.

variation of the resistivity are reported in Figure 18, whose confirm the dynamics observed in the previous year. Even if the recharge effects were slightly lower in 2022 than in 2021, resistivity models appear more homogeneous and free of sharp variations far from the drainpipe. Twenty to forty percentage resistivity increase was measured at S1 and S2, respectively, near the drainpipe. The resistivity was ~5.0 Ωm on 6/10/2022 and ~15.0 Ωm on 8/4/2022 in S2.

3.5 | Relationships Between Boundary Conditions, Groundwater and Soil Water Variables: PCA

The PCA (Figure 19, Table 4) performed on the dataset 2019–2020, 2021 and 2022 highlights that most of the variability is explained by three to four principal components. All three PCA analyses resulted in the common identification of (i) a principal component related to saltwater intrusion and (ii) one or two principal components related to boundary conditions and freshwater recharge. Principal Component 1 (PC1) is mainly related to groundwater characteristics and saltwater intrusion and represents the highest variability percentage (43% in 2019–2020, 38% in 2021 and 40% in 2022). In the three analyses, PC1 is the linear combination of groundwater EC_w, and the ions Cl^-, Na^+, K^+, Br^- (Table 4), including SO_4^{2-} and Mg^{2+} in 2021 and 2022. Moreover, depth to the water table is also negatively correlated to PC1 in 2019–2020 and 2022. Ca^{2+} is never related to PC1, but contributes to the variability of PC2 in 2019–2020 and 2021, and PC3 in 2022. Moreover, Ca^{2+} is always associated with EC_p. In 2019–2020, before the freshwater recharge, the effect of the Morto channel salinity is represented by PC3 which accounts for 14% of the dataset variability. In 2021, when the freshwater recharge lasts for 36 days, the effect of the Morto channel EC_w and the flow rate are split into two components: PC2 includes EC_w at MC3 and drain flow rate that are positively and negatively correlated to the component, respectively, while PC3 includes EC_w at MC1 and rainfall. PC2 and PC3 account for 26% of 2021 variability. Differently, in 2022, when the freshwater recharge lasts for 69 days, all the variables related to the freshwater recharge and the Morto channel salinity are included in PC2 which accounts for 22% of the total variability.

The effect of the components on the monitoring locations is shown in Figure 19a,c,e. The effect of groundwater salinity and saltwater intrusion is evident on S5 which is mainly related to PC1 in all three datasets. Moreover, its effect is predominant on S1, the closest to watercourses and lagoon (Figure 3), before the freshwater recharge and in 2022. S2 and S3, located along the sandy paleochannel, are mainly related to PC2 (i.e., soil salinity and groundwater ions like SO_4^{2-} and Ca^{2+}) and PC4 (i.e., WC_a, ET_e, rain) in 2019–2020, while the effect of the freshwater recharge, included in PC2 (Table 4), influences those locations in 2021 and especially in 2022. Indeed, the stronger effect of the draining activity is evident in 2022 when PC2 is related to all the monitoring stations including S4 and S5 located outside the drain path. S4 is not clearly discriminated by the principal components. Its variability is partially due to PC4 in 2019–2020, PC4 and PC2 in 2021 and PC1 and PC2 in 2022.

4 | Discussion

In this study, a mitigation strategy against saltwater intrusion was tested over 4 years in a coastal low-lying agricultural area

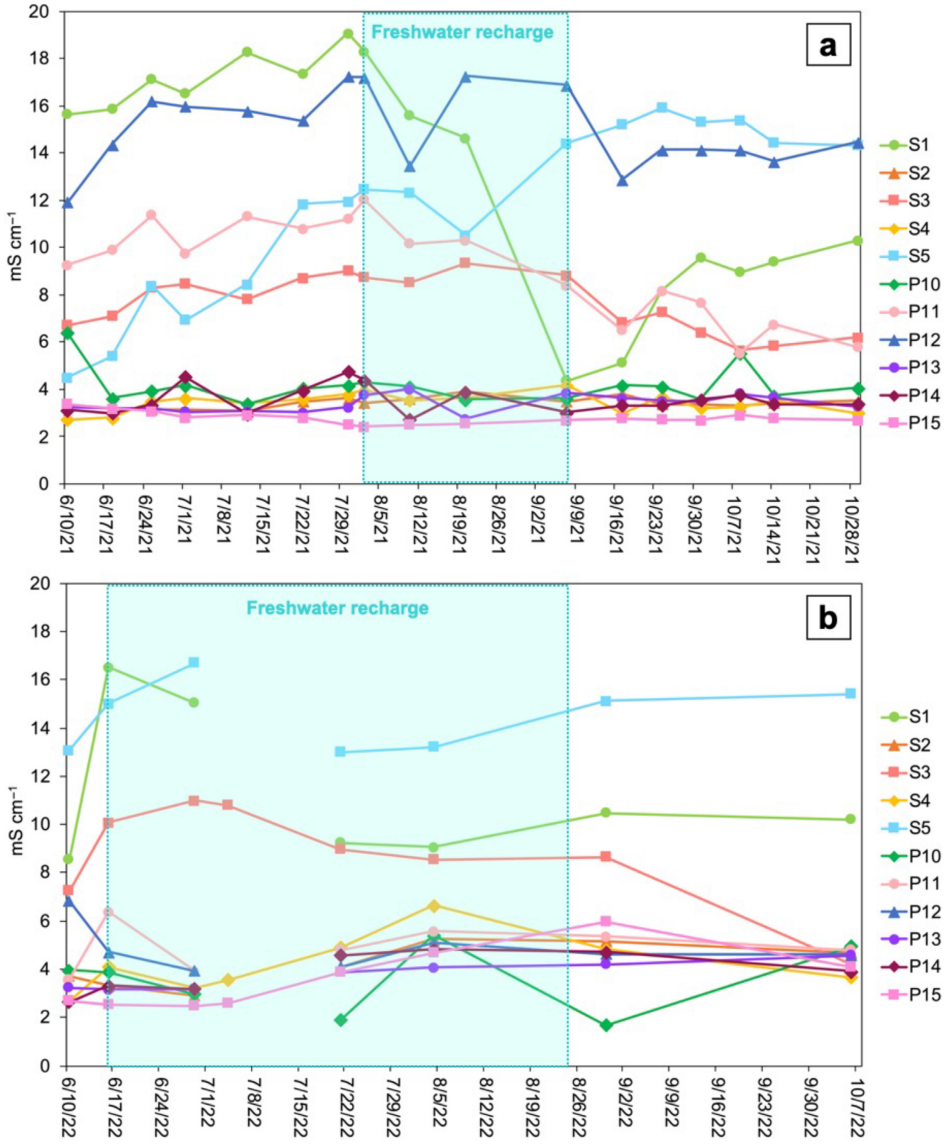

FIGURE 14 | Groundwater EC_w measured at the monitoring locations during the 2021 and 2022 cropping seasons.

TABLE 3 | Spearman's correlations (ρ) between groundwater EC_w (mS cm^{-1}) and Cl^-, SO_4^-, Na^+ (mg L^{-1}) ion concentrations measured in 2021 (blue cells) and 2022 (green cells).

	ECw	Cl^-	SO_4^{2-}	Na^+
ECw	1.00	**0.92**	**0.58**	**0.88**
Cl^-	**0.92**	1.00	**0.49**	**0.94**
SO_4^{2-}	**0.58**	**0.49**	1.00	**0.46**
Na^+	**0.88**	**0.94**	**0.46**	1.00

Note: Values range from −1 to +1 with larger absolute values indicating a stronger relationship. Bold values indicate a significant correlation ($\alpha = 0.05$).

near the Venice lagoon, Italy. After 2 years of hydrologic characterisation of the field site, an experimental infrastructure was established. It consists of a drainpipe that was installed along a sandy paleochannel crossing the silty-peat farmland. The drainpipe derives freshwater from the Morto channel and conveys it into the field. Two freshwater recharge phases were conducted during the 2021 and 2022 maize cropping seasons and the effects of the freshwater recharge were monitored in terms of soil and water electrical conductivity, water content, depth to the water table, groundwater ions and TL-ERT acquisitions. The hydrologic boundary conditions, including the salinity of the surficial waters and the weather conditions, were monitored throughout the entire study period from 2019 to 2022.

4.1 | Saltwater Dynamics During the Monitoring Period

The monitoring of EC_w in surficial waters confirms that Brenta and Bacchiglione rivers are affected by SWI for a large portion of the water profile as already stated by Carbognin et al. (2010) and Da Lio et al. (2015). The variability among dates (Figures 6 and 7) is caused by multiple factors, including the river discharge, the tidal regime and the meteorological conditions. The exceptionally scarce rainfall and high temperatures recorded in 2022 had strong consequences on the

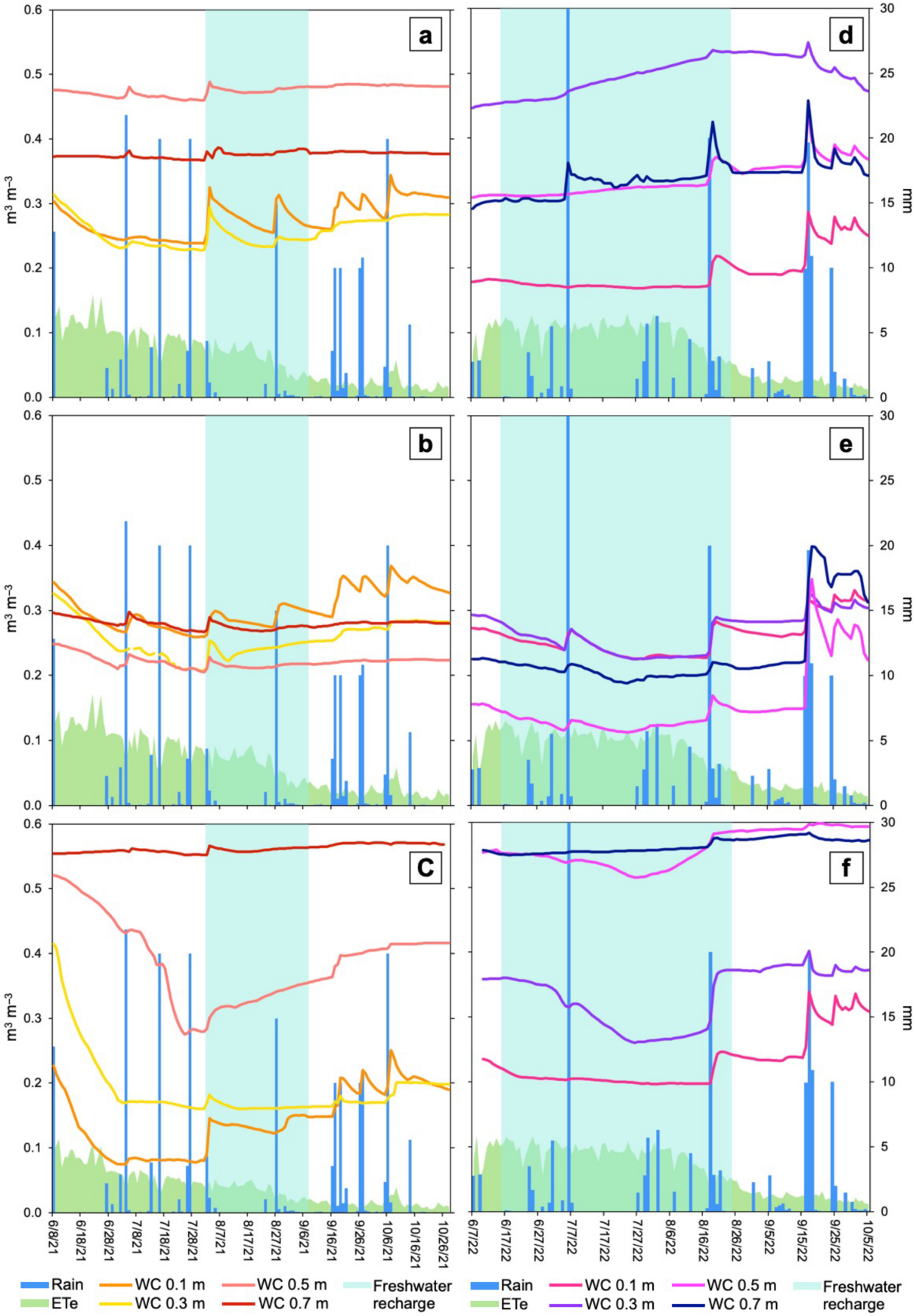

FIGURE 15 | Water content recorded in (left) 2021 and (right) 2022 at 0.1, 0.3, 0.5 and 0.7 m depths in S1 (a, d), S3 (b, e) and S5 (c, f). The panels also provide the behaviour vs. time of the daily rainfall and ET_e.

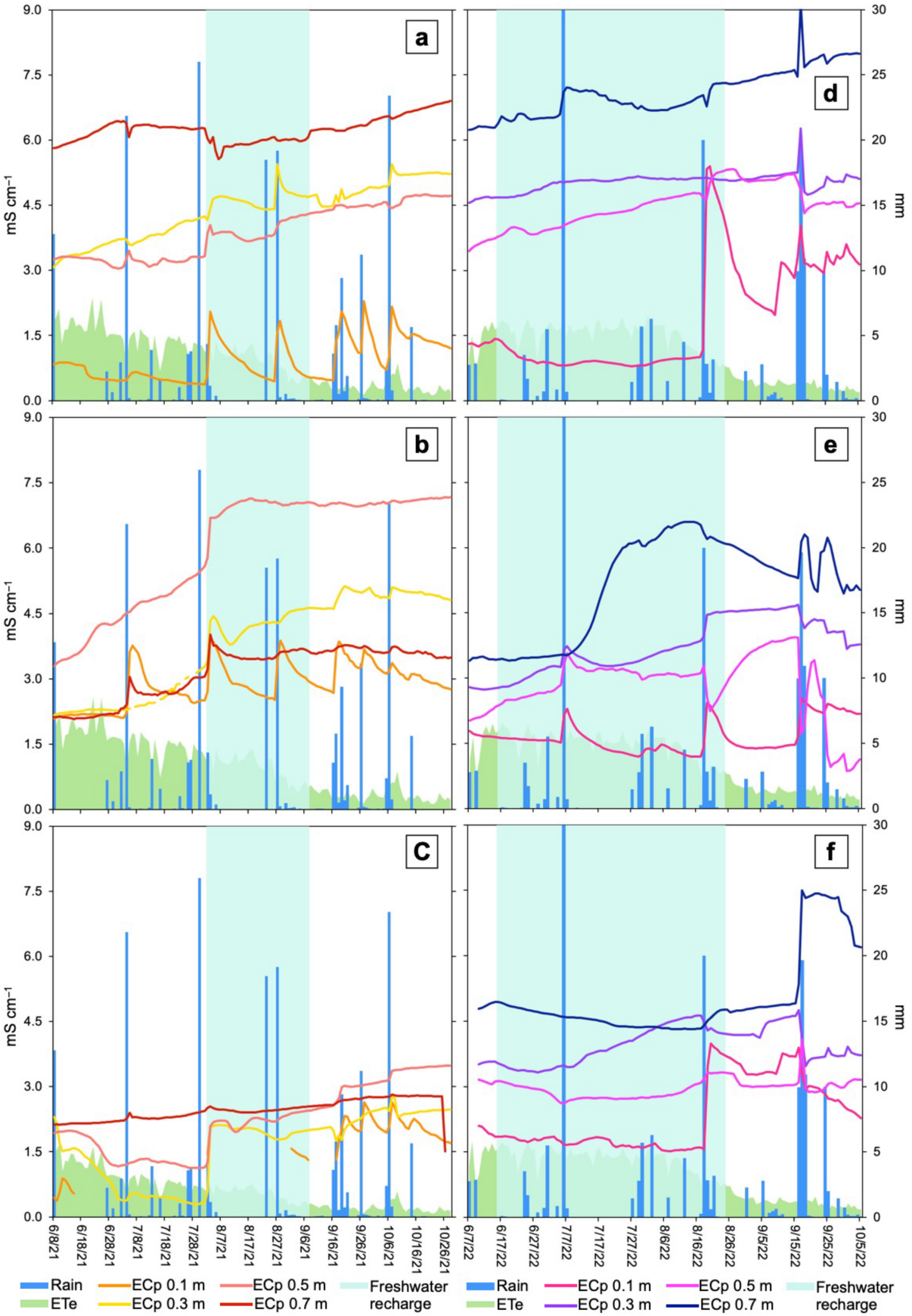

FIGURE 16 | Pore water electrical conductivity as recorded in 2021 and 2022 at 0.1, 0.3, 0.5 and 0.7 m depths in S1 (a, d), S3 (b, e) and S5 (c, f). The panels also provide the behaviour versus time of the daily rainfall and ET_e.

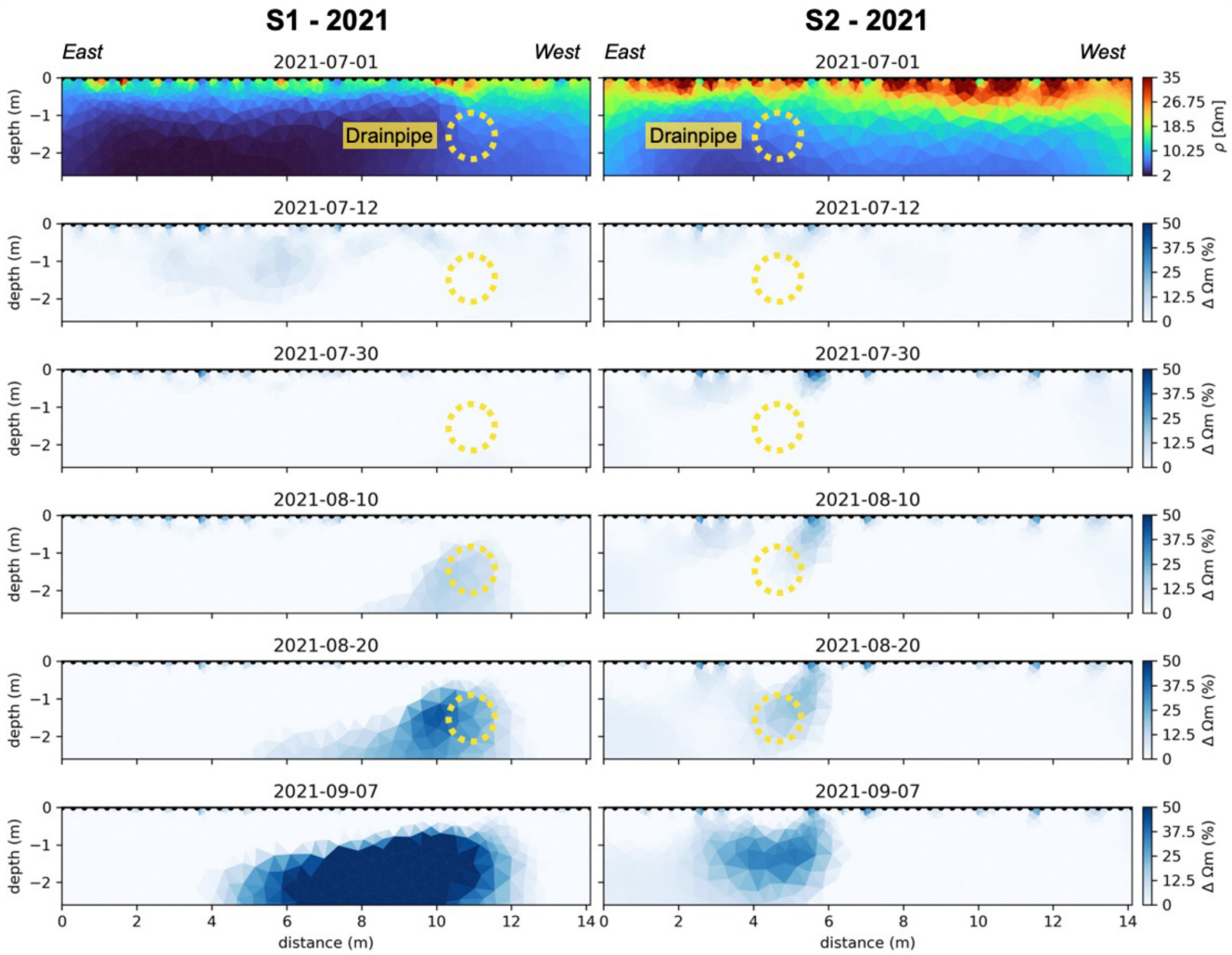

FIGURE 17 | TL-ERT profiles crossing S1 and S2 monitoring sites acquired in 2021. The outcomes are represented in terms of resistivity percentage difference between adjacent dates. The dates 7/1/2021, 7/12/2021 and 7/30/2021 represent the condition before the freshwater recharge that started on 8/2/2021 and ended on 9/7/2021.

surficial water condition. The water scarcity upstream caused a strong reduction in the freshwater flow downstream with the consequent strengthening of the encroachment from the Venice Lagoon and the Adriatic Sea. Locally, the effect was the salinization of the whole river profiles in 2022, while from 2019 to 2021 the top 2 m were almost fresh. The highest difference between monitoring years was observed in Bacchiglione river where the bottom EC_w was < 20 mS cm^{-1} from 2019 to 2021 and larger than 50 mS cm^{-1} in 2022. The Morto channel monitoring at the drain intake (MC2, Figure 3) performed in 2022 highlighted a strong salinization of its bottom (Figure 8) probably due to the increase in the salinity of the water pumped from the agricultural area.

The 2019 and 2020 monitoring campaigns and the statistical analyses confirmed that the experimental site is strongly affected by salt contamination as already highlighted by De Franco et al. (2009), Scudiero et al. (2013) and Zancanaro et al. (2020). The three monitoring sites S1, S2 and S3, located in the sandy paleochannel, were characterised by a slightly brackish top 1 m of groundwater. Despite this, the Cl/Br molar ratio highlights that salinity in S1 (i.e., the site closer to the lagoon) originated from seawater. On the contrary, the salinity of S2 and S3 is mainly soil-driven (Figure 10). The PCA (Table 4, Figure 19a,b) confirms these results highlighting that the variability of S1 is explained by PC1, the component related to SWI and groundwater salinity, while S2 and S3 variability is explained by mineral soil-driven water quality (Ca^{2+}, SO_4^{2-} and EC_p), soil water content, ET_e and rainfall. These results agree with those in Zancanaro et al. (2020) who showed how, in the same experimental site, the areas characterised by higher sand percentage, higher bulk density and low SOC, are also characterised by low salinity, because of high percolation and low CEC. Outside the paleochannel, S4 was almost fresh, while S5 was saline. Considering that S5 was also characterised by a peaty layer with very high SOC and CEC (Table 1), the salinity may be caused by the percolation of the high quantity of salts retained by the peat layer. This is confirmed by Cl/Br value higher than the seawater one which means that there was an additional source of Cl^-.

A significant deterioration in salinization conditions was observed soon after the drainpipe establishment. Comparing the monitoring periods 2019–2020 and 2021–2022, an EC_w increase up to 80% was observed and the Cl/Br molar ratio was almost

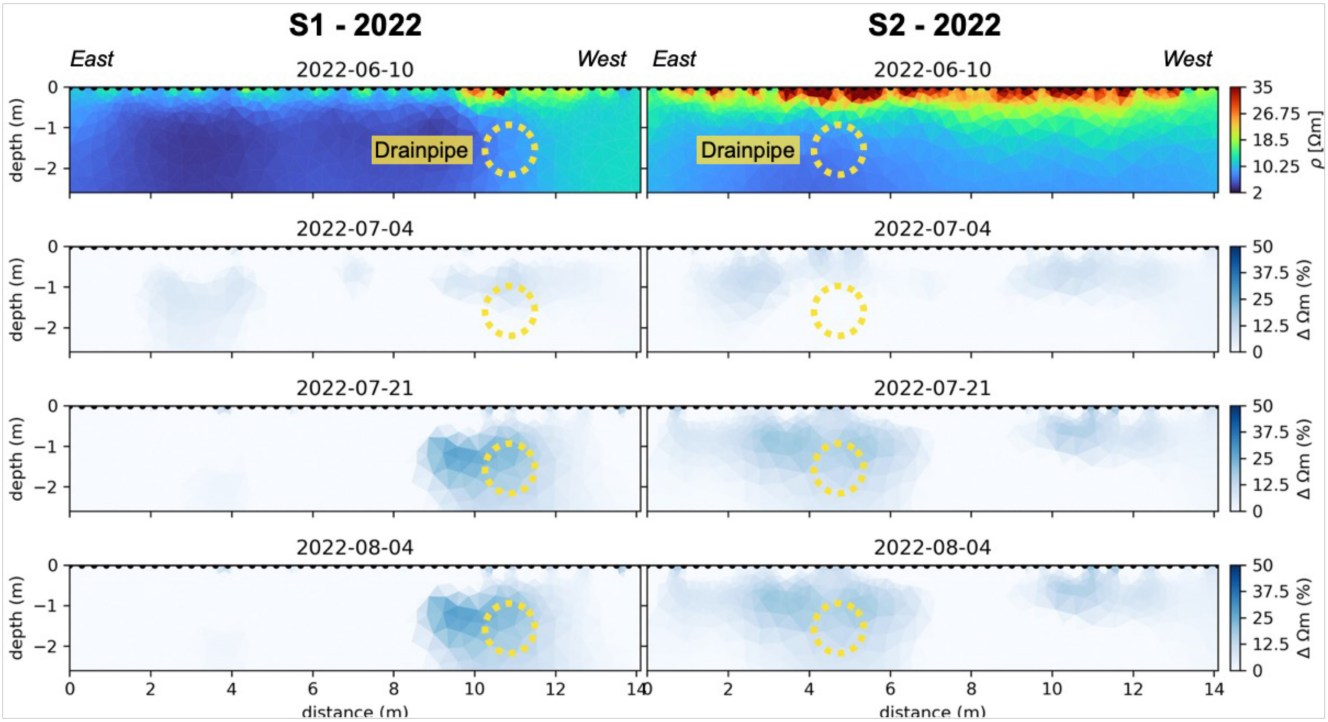

FIGURE 18 | TL-ERT profiles crossing S1 and S2 monitoring sites acquired in 2022. The outcomes are represented in terms of resistivity percentage difference between adjacent dates. One acquisition was performed before and three after the beginning of the freshwater recharge that started on 6/16/2022.

equal to the seawater value (Figure 13). The high positive significant correlations between EC_w, Cl^- and Na^+ (Tables 2 and 3) confirm that the salinity was mainly associated with seawater. Given that saltwater migration is relatively slow (De Franco et al. 2009), a sudden shift in the saltwater plume is unlikely. It is quite possible that the excavation work brought to the surface the saline water that characterises the salt-contaminated aquifer located above the freshwater lens (Cavallina et al. 2022).

4.2 | The Experimental Infrastructure and the Freshwater Recharge

The most evident effect of the freshwater recharge was observed in groundwater, especially in 2021 (Figure 17). At S1, the EC_w decreased by 75% and the TL-ERT acquisitions showed an enlargement of a more resistive volume around the drainpipe during the injection phase associated with the freshwater flow in the subsurface, while there is a general worsening (resistivity decrease) of the soil condition far from the drainpipe. This confirms the findings of Velstra, Groen, and De Jong (2011) who previously demonstrated the influence of drainpipes and ditches in draining away brackish water by using TL-ERT. Similar trends are also evident on the TL-ERT section through S2, despite EC_w in piezometer S2 remained unchanged over the injection period, being always ~3 mS cm^{-1}. It is worth noting that the injected water was characterised by a EC_w averaging 2 mS cm^{-1}, that is differing not significantly from the shallow groundwater EC_w in this site. ERT confirmed to be a non-invasive and cost-effective geophysical technique able to capture saline water intrusion spatial variability due to the peculiar sensitivity to the electrical conductivity of pore fluids which typically results in a strong contrast between fresh- and saltwater (Goebel, Pidlisecky, and Knight 2017; Águila et al. 2022; Hermans and Paepen 2020; Panthi et al. 2022). A comparison between the well location and the lateral extent of the paleochannel (Figure 4), allows to conclude that the positive effect of the freshwater recharge involved the whole paleochannel but did not laterally extend further. These results are confirmed by the PCA: the freshwater recharge associated to PC2 contributes to the variability of the monitoring sites along the paleochannel (primarily S2 and S3) and only partially to S1 and S4 (Figure 19c). Moreover, similarly to the results obtained for the 2019–2020 dataset, the PCA confirms that the salinity of S2 and S3 is mainly soil-driven as PC2 is also associated with Ca^{2+} concentration (El Moujabber et al. 2006; Zancanaro et al. 2020). On the contrary, S5 is not affected by the recharge effect and its variability is related to the saltwater intrusion component (PC1).

Similar results were also found in 2022 (Figure 18), although the beneficial effects of the freshwater recharge were less evident, particularly in the TL-ERT section. This was likely due to multiple factors: (i) the 2022 exceptional weather conditions that caused a worsening of the salinization of the shallow groundwater water; and (ii) the higher EC_w of the Morto channel. Notice that the water discharged by the drainpipe was sporadically saltier than the groundwater (cfr Figures 11 and 14). Despite this, the PCA (Figure 19e,f) highlights that the principal component related to the freshwater recharge completely explains the variability of S2 and S3, and partially of S1, S4 and S5 where PC1, related to saltwater intrusion, is predominant. This means that the water recharge reached all the monitoring sites along the paleochannel and was also able to spread laterally. Despite this, the

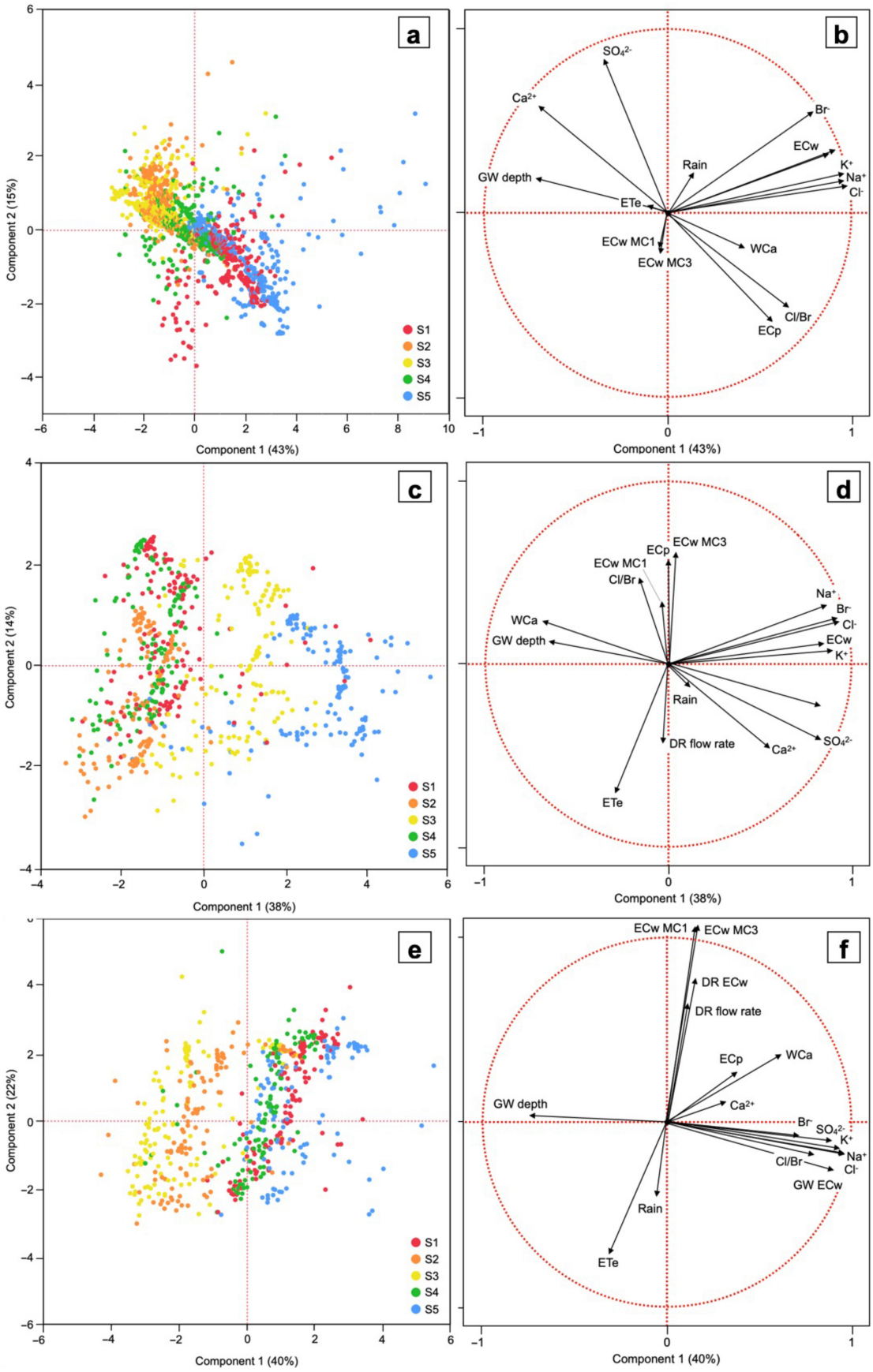

FIGURE 19 | PCA results for three datasets 2019–2020, 2021 and 2022. (a, c and e) Show the PCA score plot for PC1 and PC2. Each colour represents a monitoring location (S1 to S5). (b, d and f) show the loading plots representing the factor loadings for PC1 and PC2. GW stands for groundwater and DR for drain.

TABLE 4 | PCA of the three datasets 2019–2020, 2021 and 2022 with the variables related to each principal component (PC), the variability percentage explained by each variable, and their positive (+) or negative (–) correlation with the PC.

	2019–2020			2021			2022		
	Variable	**%**	**+/–**	**Variable**	**%**	**+/–**	**Variable**	**%**	**+/–**
PC1	GW EC_w	11	+	GW EC_w	11	+	GW EC_w	10	+
	Cl^-	13	+	Cl^-	13	+	Cl^-	12	+
	Na^+	13	+	Na^+	13	+	Na^+	12	+
	K^+	13	+	K^+	12	+	K^+	11	+
	Br^-	12	+	Br^-	13	+	Br^-	7	+
	GW depth	7	–				GW depth	7	–
				SO_4^{2-}	10	+	SO_4^{2-}	10	+
				Mg^{2+}	10	+	Mg^{2+}	12	+
				WC_a	7	–			
							Cl/Br	8	+
PC2	SO_4^{2-}	28	+						
	Mg^{2+}	12	+						
	Ca^{2+}	14	+	Ca^{2+}	9	–			
	Cl/Br	11	–	Cl/Br	9	+			
	EC_p	14	–	EC_p	13	+			
				EC_w MC3	15	+	EC_w MC3	26	+
				DR flow rate	8	–	DR flow rate	9	+
							DR EC_w	14	+
							EC_w MC1	26	+
							ET_e	11	–
PC3	EC_w MC3	38	+						
	EC_w MC1	39	+	EC_w MC1	33	–			
				Rain	30	+	Rain	23	+
							WC_a	8	+
							EC_p	10	+
							Ca^{2+}	23	+
PC4	ET_e	37	+	ET_e	21	+			
	WC_a	36	–						
	Rain	9	–						
				GW depth	8	+			

Abbreviations: GW, groundwater; DR, drain.

factors listed above limited the beneficial effect of the recharge and the saltwater intrusion remained the major factor influencing the monitoring sites S1, S4 and S5.

This study confirms that the aquifer artificial recharge with freshwater is an efficient method for SWI limitation (Hussain et al. 2019). The injection of freshwater through a buried drain has been proven to be a considerable alternative to the use of injection wells. However, the huge initial cost of the infrastructure should be considered a limitation. In addition, further studies are needed to verify the efficacy of the studied countermeasure in the improvement of the agricultural productivity of the area. Considering the most effective strategies against SWI (Hussain et al. 2019; Saad et al. 2023), the studied countermeasure may be

associated with alternative approaches. For example, the huge amount of salty/brackish water pumped from the agricultural area may be considered as an alternative source of water to be used as a hydraulic barrier after a desalinization treatment.

5 | Conclusions

In conclusion, the study confirms that the freshwater recharge from an artificial channel exploiting the high permeability of a sandy paleochannel is effective in reducing the groundwater salinity, although no evidence was found for soil water. Considering that the beneficial effects should enhance the agricultural productivity of the area, additional studies should deepen this aspect to verify if the freshwater recharge effects limited to groundwater are enough to reach this goal. In addition, the installation of one drainpipe limited the effect of the freshwater recharge to a narrow area, so an implementation with the installation of a drainpipe network should be considered. Finally, climate change is going to worsen SWI, increase temperatures and lower rainfall events, with extreme climate conditions as observed in 2022. Thus, further studies and analyses should be implemented to verify if the beneficial effects are worth the huge initial work and cost.

Acknowledgements

This work was supported by the EU co-financing and the Interreg Italy–Croatia Cross Border Collaboration (CBC) Programme 2014–2020 (Priority Axes: Safety and Resilience) through the European Regional Development Fund as a part of the projects 'Monitoring sea-water intrusion in coastal aquifers and testing pilot projects for its mitigation' (MoST, AID: 10047742) and 'Salt- water intrusion and climate change: monitoring, countermeasures and informed governance' (SeCure, AID: 10419304). This study was also carried out within the RETURN Extended Partnership and received funding from the European Union Next-GenerationEU (National Recovery and Resilience Plan—NRRP, Mission 4, Component 2, Investment 1.3—D.D. 1243 2/8/2022, PE.0000005). Open access publishing facilitated by Universita degli Studi di Padova, as part of the Wiley - CRUI-CARE agreement.

Data Availability Statement

The data that support the findings of this study are available on request from the corresponding author. The data are not publicly available due to privacy or ethical restrictions.

References

Águila, J. F., M. C. McDonnell, R. Flynn, et al. 2022. "Characterizing Groundwater Salinity Patterns in a Coastal Sand Aquifer at Magilligan, Northern Ireland, Using Geophysical and Geotechnical Methods." *Environment and Earth Science* 81: 231. https://doi.org/10.1007/s12665-022-10357-1.

Alcalá, F. J., and E. Custodio. 2008. "Using the Cl/Br Ratio as a Tracer to Identify the Origin of Salinity in Aquifers in Spain and Portugal." *Journal of Hydrology* 359: 189–207. https://doi.org/10.1016/j.jhydrol.2008.06.028.

Alessandrino, L., M. Gaiolini, F. A. Cellone, et al. 2023. "Salinity Origin in the Coastal Aquifer of the Southern Venice Lowland." *Science of the Total Environment* 905: 167058. https://doi.org/10.1016/J.SCITOTENV.2023.167058.

Allen, R. G., L. S. Pereira, D. Raes, and M. Smith. 1998. *Crop Evapotranspiration. Guidelines for Computing Crop Water Requirements*; FAO Irrigation and Drainage Paper No. 56. Rome, Italy: FAO.

Bartlett, M. S. 1951. "The Effect of Standardization on a $\chi 2$ Approximation in Factor Analysis." *Biometrika* 38, no. 3/4: 337–344.

Binley, A., A. Ramirez, and W. Daily. 1995. "Regularized Image Reconstruction of Noisy Electrical Resistance Tomography Data." In *Proceedings of the 4th Workshop of the European Concerted Action on Process Tomography*, edited by M. S. Beck, B. S. Hoyle, M. A. Morris, R. C. Waterfall, and R. C. Williams, 401–410. Bergen, Norway.

Bittelli, M., M. C. Andrenelli, G. Simonetti, et al. 2019. "Shall We Abandon Sedimentation Methods for Particle Size Analysis in Soils?" *Soil and Tillage Research* 185: 36–46. https://doi.org/10.1016/j.still.2018.08.018.

Carbognin, L., P. Teatini, A. Tomasin, and L. Tosi. 2010. "Global Change and Relative Sea Level Rise at Venice: What Impact in Term of Flooding." *Climate Dynamics* 35: 1039–1047. https://doi.org/10.1007/s00382-009-0617-5.

Cavallina, C., A. Bergamasco, M. Cosma, et al. 2022. "Morpho-Sedimentary Constraints in the Groundwater Dynamics of Low-Lying Coastal Area: The Southern Margin of the Venice Lagoon, Italy." *Water* 14: 2717. https://doi.org/10.3390/w14172717.

Da Lio, C., E. Carol, E. Kruse, P. Teatini, and L. Tosi. 2015. "Saltwater Contamination in the Managed Low-Lying Farmland of the Venice Coast, Italy: An Assessment of Vulnerability." *Science of the Total Environment* 533: 356–369. https://doi.org/10.1016/j.scitotenv.2015.07.013.

De Franco, R., G. Biella, L. Tosi, et al. 2009. "Monitoring the Saltwater Intrusion by Time Lapse Electrical Resistivity Tomography: The Chioggia Test Site (Venice Lagoon, Italy)." *Journal of Applied Geophysics* 69: 117–130. https://doi.org/10.1016/j.jappgeo.2009.08.004.

El Moujabber, M., B. Bou Samra, T. Darwish, and T. Atallah. 2006. "Comparison of Different Indicators for Groundwater Contamination by Seawater Intrusion on the Lebanese Coast." *Water Resources Management* 20: 161–180. https://doi.org/10.1007/s11269-006-7376-4.

Falls, W. F., C. Ransom, J. E. Landmeyer, E. J. Reuber, and L. E. Edwards. 2005. "Hydrogeology, Water Quality, and Saltwater Intrusion in the Upper Floridan Aquifer in the Offshore Area Near Hilton Head Island, South Carolina, and Tybee Island, Georgia." *Scientific Investigations Report* 1999-2002: 2005–5134.

FAO-UNESCO. 1989. "Soil Map of the World, Revised Legend." Food and Agriculture Organization of the United Nations.

Goebel, M., A. Pidlisecky, and R. Knight. 2017. "Resistivity Imaging Reveals Complex Pattern of Saltwater Intrusion Along Monterey Coast." *Journal of Hydrology* 551: 746–755. https://doi.org/10.1016/j.jhydrol.2017.02.037.

Greenacre, M., P. J. F. Groenen, T. Hastie, A. Iodice D'Enza, A. Markos, and E. Tuzhilina. 2022. "Principal Component Analysis." *Nature Reviews Methods Primers* 2: 100. https://doi.org/10.1038/s43586-022-00184-w.

Grossman, R. B., and T. G. Reinsch. 2002. "Bulk Density and Linear Extensibility." In *Methods of Soil Analysis Part 4 Physical Methods*, edited by J. H. Dane and G. C. Topp, 201–228. Madison, WI: Soil Science Society of America Inc.

Hermans, T., and M. Paepen. 2020. "Combined Inversion of Land and Marine Electrical Resistivity Tomography for Submarine Groundwater Discharge and Saltwater Intrusion Characterization." *Geophysical Research Letters* 47, no. 3: e2019GL085877. https://doi.org/10.1029/2019GL085877.

Hilhorst, M. A. 2000. "A Pore Water Conductivity Sensor." *Soil Science Society of America Journal* 64, no. 6: 1922–1925. https://doi.org/10.2136/sssaj2000.6461922x.

Hussain, M. S., H. F. Abd-Elhamid, A. A. Javadi, and M. M. Sherif. 2019. "Management of Seawater Intrusion in Coastal Aquifers: A Review." *Water* 11: 2467. https://doi.org/10.3390/w11122467.

IPCC. 2023. "Climate Change 2023: Synthesis Report." In *Contribution of Working Groups I, II and III to the Sixth Assessment Report of the Intergovernmental Panel on Climate Change*, edited by H. Lee and J. Romero, 35–115. Geneva, Switzerland: IPCC.

Ketabchi, H., D. Mahmoodzadeh, B. Ataie-Ashtiani, and C. T. Simmons. 2016. "Sea-Level Rise Impacts on Seawater Intrusion in Coastal Aquifers: Review and Integration." *Journal of Hydrology* 535: 235–255. https://doi.org/10.1016/j.jhydrol.2016.01.083.

Kim, J. H., M. J. Yi, S. G. Park, and J. G. Kim. 2009. "4-D Inversion of DC Resistivity Monitoring Data Acquired Over a Dynamically Changing Earth Model." *Journal of Applied Geophysics* 68, no. 4: 522–532. https://doi.org/10.1016/j.jappgeo.2009.03.002.

Manoli, G., S. Bonetti, E. Scudiero, et al. 2006. "Monitoring and Modeling Farmland Productivity Along the Venice Coastland, Italy." *Procedia Environmental Sciences* 19: 361–368. https://doi.org/10.1016/j.proenv.2013.06.041.

Millero, F. J., R. Feistel, D. G. Wright, and T. J. McDougall. 2008. "The Composition of Standard Seawater and the Definition of the Reference-Composition Salinity Scale." *Deep-Sea Res. Part I* 55: 50–72. https://doi.org/10.1016/j.dsr.2007.10.001.

Motallebian, M., H. Ahmadi, A. Raoof, and N. Cartwright. 2019. "An Alternative Approach to Control Saltwater Intrusion in Coastal Aquifers Using Surface Recharge Canal." *Journal of Contaminant Hydrology* 222: 56–64. https://doi.org/10.1016/j.jconhyd.2019.02.007.

Mulligan, A. E., R. L. Evans, and D. Lizarralde. 2007. "The Role of Paleochannels in Groundwater/Seawater Exchange." *Journal of Hydrology* 335: 313–329. https://doi.org/10.1016/j.jhydrol.2006.11.025.

Oude Essink, G. H. P. 2001. "Improving Fresh Groundwater Supply–Problems and Solutions." *Ocean and Coastal Management* 44: 429–449. https://doi.org/10.1016/S0964-5691(01)00057-6.

Panthi, J., S. M. Pradhanang, A. Nolte, and T. B. Boving. 2022. "Saltwater Intrusion Into Coastal Aquifers in the Contiguous United States - A Systematic Review of Investigation Approaches and Monitoring Networks." *Science of the Total Environment* 836: 155641. https://doi.org/10.1016/j.scitotenv.2022.155641.

Prusty, P., and S. H. Farooq. 2020. "Seawater Intrusion in the Coastal Aquifers of India - A Review." *HydroResearch* 3: 61–67. https://doi.org/10.1016/j.hydres.2020.06.001.

Rasmussen, P., T. O. Sonnenborg, G. Goncear, and K. Hinsby. 2013. "Assessing Impacts of Climate Change, Sea Level Rise, and Drainage Canals on Saltwater Intrusion to Coastal Aquifer." *Hydrology and Earth System Sciences* 17: 421–443. https://doi.org/10.5194/hess-17-421-2013.

Rücker, C., T. Günther, and F. M. Wagner. 2017. "pyGIMLi: An Open-Source Library for Modelling and Inversion in Geophysics." *Computational Geosciences* 109: 106–123. https://doi.org/10.1016/j.cageo.2017.07.011.

Saad, S., A. A. Javadi, H. F. Abd-Elhamid, and H. Farmani. 2023. "Mitigating Seawater Intrusion in Coastal Aquifers: Novel Approach With Treated Wastewater Injection and Groundwater Circulation." *Journal of Hydrology* 626: 130139. https://doi.org/10.1016/j.jhydrol.2023.130139.

Sabattini, J. A., and R. A. Sabattini. 2021. "Rainfall Trends in Humid Temperate Climate in South America: Possible Effects in Ecosystems of Espinal Ecoregion." In *The Nature, Causes, Effects and Mitigation of Climate Change on the Environment*, edited by S. A. Harris. London, UK: IntechOpen. https://doi.org/10.5772/intechopen.99080.

Samadder, R., S. Kumar, and R. P. Gupta. 2011. "Paleochannels and Their Potential for Artificial Groundwater Recharge in the Western Ganga Plains." *Journal of Hydrology* 400: 154–164. https://doi.org/10.1016/j.jhydrol.2011.01.039.

Scudiero, E., P. Teatini, D. L. Corwin, R. Deiana, A. Berti, and F. Morari. 2013. "Delineation of Site-Specific Management Units in a Saline Region at the Venice Lagoon Margin, Italy, Using Soil Reflectance and Apparent Electrical Conductivity." *Computers and Electronics in Agriculture* 99: 54–64. https://doi.org/10.1016/j.compag.2013.08.023.

Tosi, L., C. Da Lio, A. Bergamasco, et al. 2022. "Sensitivity, Hazard, and Vulnerability of Farmlands to Saltwater Intrusion in Low-Lying Coastal Areas of Venice, Italy." *Water* 14: 64. https://doi.org/10.3390/W14010064.

Velstra, J., J. Groen, and K. De Jong. 2011. "Observations of Salinity Patterns in Shallow Groundwater and Drainage Water From Agricultural Land in the Northern Part of The Netherlands." *Irrigation and Drainage* 60, no. S1: 51–58. https://doi.org/10.1002/ird.675.

Wagner, F. M., and S. Uhlemann. 2021. "An Overview of Multimethod Imaging Approaches in Environmental Geophysics." *Advances in Geophysics* 62, no. 3: 1–72. https://doi.org/10.1016/bs.agph.2021.06.001.

Werner, A. D., M. Bakker, V. E. A. Post, et al. 2013. "Seawater Intrusion Processes, Investigation and Management: Recent Advances and Future Challenges." *Advances in Water Resources* 51: 3–26. https://doi.org/10.1016/j.advwatres.2012.03.004.

Wilkinson, P. B., J. E. Chambers, P. I. Meldrum, et al. 2022. "Windowed 4D Inversion for Near Real-Time Geoelectrical Monitoring Applications." *Frontiers in Earth Science* 10: 983603. https://doi.org/10.3389/feart.2022.983603.

Zancanaro, E., P. Teatini, E. Scudiero, and F. Morari. 2020. "Identification of the Origins of Vadose-Zone Salinity on an Agricultural Site in the Venice Coastland by Ionic Molar Ratio Analysis." *Water* 12: 3363. https://doi.org/10.3390/w12123363.

Supporting Information

Additional supporting information can be found online in the Supporting Information section.